Aus der Klinik und Poliklinik für Frauenheilkunde und Geburtshilfe
der Universität zu Köln
Direktor: Universitätsprofessor Dr. med. P. K. Mallmann

Effects of scrotal hyperthermia on inducing signaling pathways of Alkaliptosis and Oxeiptosis in testicular tissue of adult male mice

Inaugural-Dissertation zur Erlangung der Doktorwürde
der Medizinischen Fakultät
der Universität zu Köln

vorgelegt von
Sara Omrani
aus Tabriz, Iran

promoviert am 09. Dezember 2025

Gedruckt mit Genehmigung der Medizinischen Fakultät der Universität zu Köln

2026

Dekan: Universitätsprofessor Dr. med. G. R. Fink

1. Gutachterin: Professorin Dr. med. G. Rahimi
2. Gutachter: Universitätsprofessor Dr. rer. nat. H. Kashkar

Erklärung

Ich erkläre hiermit, dass ich die vorliegende Dissertationsschrift ohne unzulässige Hilfe Dritter und ohne Benutzung anderer als der angegebenen Hilfsmittel angefertigt habe; die aus fremden Quellen direkt oder indirekt übernommenen Gedanken sind als solche kenntlich gemacht.

Bei der Auswahl und Auswertung des Materials sowie bei der Herstellung des Manuskriptes habe ich keine Unterstützungsleistung erhalten.

Weitere Personen waren an der geistigen Herstellung der vorliegenden Arbeit nicht beteiligt. Insbesondere habe ich nicht die Hilfe einer Promotionsberaterin oder eines Promotionsberaters in Anspruch genommen. Dritte haben von mir weder unmittelbar noch mittelbar geldwerte Leistungen für Arbeiten erhalten, die im Zusammenhang mit dem Inhalt der vorgelegten Dissertationsschrift stehen.

Die Dissertationsschrift wurde von mir bisher weder im Inland noch im Ausland in gleicher oder ähnlicher Form einer anderen Prüfungsbehörde vorgelegt.

Ein Teil dieser Arbeit wurde im Rahmen einer wissenschaftlichen Zusammenarbeit an der Shahid Beheshti Universität für Medizinwissenschaften in Teheran (Iran) durchgeführt. Die Datenerhebung sowie die experimentellen Laborarbeiten fanden unter der Aufsicht von Prof. Mir Davood Omrani (Zweitbetreuer) statt.

Während der Durchführung der Experimente wurde ich zudem von Prof. Marefat Ghafari Novin aus der Abteilung für Reproduktionsmedizin wissenschaftlich begleitet und beraten.

Die in dieser Arbeit dargestellten Experimente wurden unter Anleitung der oben genannten Personen eigenständig von mir durchgeführt.

Die statistische Auswertung erfolgte mit Unterstützung der Abteilung für Genetik derselben Universität unter der Supervision von Prof. Mir Davood Omrani. Dabei kamen

folgende Softwareprogramme zum Einsatz: GraphPad Prism (Version 9.3.1), LinRegPCR (Version 10.1) sowie REST (Version 2008).

Erklärung zur guten wissenschaftlichen Praxis:

Ich erkläre hiermit, dass ich die Ordnung zur Sicherung guter wissenschaftlicher Praxis und zum Umgang mit wissenschaftlichem Fehlverhalten (Amtliche Mitteilung der Universität zu Köln Am 132/2020) der Universität zu Köln gelesen habe und verpflichte mich hiermit, die dort genannten Vorgaben bei allen wissenschaftlichen Tätigkeiten zu beachten und umzusetzen.

Köln, den 30.06.2025

Thanksgiving

I would like to dedicate my dissertation to my parents my beloved husband and also my dear friends. A special feeling of gratitude goes to my loving dad, whose words of encouragement and striving for perseverance ring in my ears.

Table of Contents

List of abbreviations

Lorem ipsum

SHBG	Sex Hormone Binding Globulin
HOST	Hypo-Osmotic Swelling Test score
IUR	Isotropic uniform random sampling
LSD	least significant difference
LH	Luteinizing hormone
FSH	Follicle stimulating hormone
ELISA	Enzyme-Linked Immunosorbent Assay
H&E	Hematoxylin and Eosin
DEPC	Diethyl pyro carbonate
NF-κB	Nuclear factor kappa-light-chain-enhancer of activated Beta cells
IKBKB	Inhibitor of Nuclear Factor Kappa Beta Kinase Subunit Beta
CA	Carbonic Anhydrase
Keap1	Kelch-like ECH-associated protein 1
PGAM	Phosphoglycerate mutase
AIFM1	Apoptosis Inducing Factor Mitochondria Associated 1
IT	Interstitial tissue
ATG5	Autophagy Related 5
MLKL	Mixed Lineage Kinase Domain like Pseudo kinase
ACSL4	Acyl-CoA Synthetase Long Chain Family Member 4
NHE	Sodium-Hydrogen Exchangers
ROS	Reactive oxygen species

1. Zusammenfassung and Summary

1.1. Zusammenfassung

Hintergrund: Alkaliptose und Oxeiptose sind zwei wichtige Signalwege im Rahmen der Regulierung des programmierten Zelltods, die unter anderem durch erhöhte Temperaturen aktiviert werden können. Die Alkaliptose stellt eine pH-abhängige Form des regulierten Zelltods dar, die über die Aktivierung des IKBKB-NF-κB-Signalwegs und die nachfolgende Herunterregulation von CA9 vermittelt wird. Im Gegensatz dazu handelt es sich bei der Oxeiptose um eine neu beschriebene, durch Sauerstoffradikale ausgelöste, caspase-unabhängige Form des Zelltods, die durch den KEAP1-PGAM5-AIFM1-Signalweg gesteuert wird. Ziel dieser Studie war es, den Einfluss skrotaler Hyperthermie auf die Induktion der molekularen Signalwege der Alkaliptose und Oxeiptose sowie auf das Hodengewebe und die Spermienqualität adulter männlicher Mäuse zu untersuchen.

Methode: Insgesamt wurden 20 adulte männliche Mäuse mit einem Gewicht von 25–30 g zufällig in zwei Gruppen aufgeteilt: eine Hyperthermie-Gruppe und eine Kontrollgruppe. Bei den Tieren der Hyperthermie-Gruppe wurde eine lokale Erwärmung des Hodensacks auf 43 °C für 20 Minuten durchgeführt. Am Ende des Versuchszeitraums wurden Blutproben zur Bestimmung des Serumtestosterons entnommen, und es erfolgten umfassende Spermienanalysen (Konzentration, Beweglichkeit, Lebensfähigkeit und Morphologie). Außerdem wurden histologische Untersuchungen der Hoden und Analyse nicht-apoptotischer Zellschäden durchgeführt. Die Genexpression der an den Signalwegen von Alkaliptose (IKBKB, NF-κB, CA9) und Oxeiptose (KEAP1, PGAM5, AIFM1) beteiligten Gene wurde mittels Real-Time-PCR untersucht.

Ergebnisse: In der Hyperthermie-Gruppe waren sowohl die Gesamtzahl der Spermien als auch der Anteil normal beweglicher, lebensfähiger und morphologisch intakter Spermien signifikant reduziert im Vergleich zur Kontrollgruppe ($P < 0,001$). Der Testosteronspiegel im Serum war in dieser Gruppe ebenfalls signifikant niedriger ($P < 0,001$). Zusätzlich wurden ein Rückgang des Hodenvolumens, der Länge der Samenkanälchen sowie der Anzahl testikulärer Zellen festgestellt ($P < 0,001$). Die Analyse der Genexpression ergab eine signifikante Erhöhung der relativen Expression von NF-κB ($P < 0,001$) und eine deutliche Reduktion von CA9 ($P < 0,0001$) im Alkaliptose-Signalweg. Für IKBKB konnte kein signifikanter Unterschied zwischen den Gruppen festgestellt werden. Im Oxeiptose-Signalweg zeigte AIFM1 eine signifikant verminderte

Expression in der Hyperthermie-Gruppe ($P < 0,001$), während KEAP1 und PGAM5 eine signifikante Erhöhung der relativen Expression aufwiesen ($P < 0,001$ bzw. $P < 0,0001$).

Fazit: Die Real-Time-PCR-Analyse offenbarte eine deutliche Deregulierung in den Expressionsmustern der Marker für Oxeiptose und Alkaliptose. Daraus lässt sich schließen, dass skrotale Hyperthermie nicht-apoptotischen Zelltod induzieren und die entsprechenden molekularen Signalwege aktivieren kann.

1.2. Summary

Background: Alkaliptosis and Oxeiptosis are important pathways in cell-death regulation, which can be induced by exposing to high temperature. Alkaliptosis is a pH-dependent form of regulated cell death driven by activation of the IKBKB-NF-B pathway-dependent downregulation of CA9. On the other hand, Oxeiptosis is a novel oxygen radical-induced caspase-independent regulated cell death driven by the activation of the KEAP1-PGAM5-AIFM1 pathway. The objective of this study was to examine the effects of scrotal hyperthermia on the induction of Alkaliptosis and Oxeiptosis molecular pathways, and its influence on testicular tissue and sperm analysis in adult male mice. **Method**: In the present study, 20 adult male mice weighing 25-30 g were randomly divided into two groups, a hyperthermia group and a control group. Each animal in the hyperthermia group is induced by scrotal hyperthermia at 43°C for 20 minutes. At the end of the experimental period, serum testosterone, sperm analyses including sperm concentration, motility, survival, morphology, and testicular histological studies such as stereoscopic examination and non-apoptotic cell death were performed in both groups. In addition, the expression of genes involved in the alkaliptosis (IKBKB-NF-κB and CA9) and oxeiptosis (KEAP1, PGAM5, and AIFM1) molecular pathways was analyzed using real-time PCR.

Results: In the hyperthermia group, the total sperm count and the percentage of sperm exhibiting normal motility, viability, and morphology were significantly lower than those in the control group (P<0.001). Additionally, serum testosterone measurements revealed a significant reduction in the hyperthermia group (P<0.001). Testis volume, length of seminiferous tubules, and the number of testicular cells were also significantly decreased in the hyperthermia group compared to the control group (P<0.001). Assessment of the gene expression in the Oxeiptosis and Alkaliptosis pathways revealed the following findings. In the Alkaliptosis pathway, there was a notable increase in the relative expression of NF-κB (P<0.001), while the relative expression of CA9 exhibited a significant decrease (P<0.0001) in the scrotal hyperthermia group when compared to the control group. For the *IKBKB* gene, the relative expression showed no significant difference between scrotal hyperthermia and control groups. Considering Oxeiptosis pathway, the *AIFM1* gene showed a significant decrease in the scrotal hyperthermia group compared to the control group (P<0.001). While, the relative expression of *KEAP1* and *PGAM5* genes demonstrated a significant increase (P<0.001 and P<0.0001 respectively) in the scrotal hyperthermia group compared to the control group.

Conclusion: Real-time PCR analysis revealed a remarkable deregulation in the gene expression pattern of Oxeiptosis and Alkaliptosis markers. Therefore, it can be concluded that scrotal

hyperthermia can induce non-apoptotic cell death and activate the signaling pathways associated with Oxeiptosis and Alkaliptosis.

2. Introduction

2.1. Problem statement and Review of literature

Infertility is a complex medical condition that affects both men and women. Fifty percent of couples' infertility is due to men(1,2). In mammals, the normal process of spermatogenesis requires relatively low temperatures. The temperature of the scrotum in most mammals has been shown to be 4 to 5ºC lower than the basal body temperature. Disruption of the spermatogenesis process occurs after exposure of the testicles to high temperatures, leading to the death of testicular and germinal cells(3). Cell death can occur through accidental cell death (ACD) and regulated cell death (RCD). ACD is characterized by its lack of control, whereas RCD is mediated by defined signaling pathways in response to harmful stimuli. Recent developments have led to the identification of various RCD forms, prompting a transition in the classification of cell death from a morphological to a molecular framework(4,5). Molecular frameworks have enabled the induction and inhibition of these pathways using various stressors to study their roles in medical conditions such as infertility and oligo/azoospermia. In this regard, Pirani et al. studied the effects of scrotal hyperthermia in mice on the apoptotic marker Caspase-3 and found increased levels of apoptotic activity in the scrotal hyperthermia group(6). Khosravi et al. examined the expressions of apoptotic genes, including c-Kit, Ddx-4, Caspase-3, Gfr-α, Oct-4, Plzf, and Pcna, after scrotal hyperthermia and found increased levels of apoptotic activity(7). Hasani et al. investigated the roles of non-apoptotic pathways—pyroptosis, autophagy, necroptosis, and ferroptosis—by measuring the mRNA expression levels of Caspase-1, Bcl-2, Atg7, MLkl, and Acsl4 in testis tissue after scrotal hyperthermia, and found increased levels of expression(8). Two newly discovered regulated cell death processes that are particularly independent of the caspase pathway are alkaliptosis and oxeiptosis. Alkaliptosis is a pH-dependent form of regulated cell death triggered by activation of the IKBKB-NF-κB and CA9 signaling pathway. Oxeiptosis is a novel oxygen radical-induced caspase-independent regulated cell death driven by the activation of the KEAP1-PGAM5-AIFM1 pathway(4,5,9,10). There is lack of research on role of newer discovered programmed cell death pathways specifically caspase independent pathways like alkaliptosis and oxeiptosis. Therefore, the aim of the present study was to determine the effects of scrotal hyperthermia on the induction of oxeiptosis and alkaliptosis signaling pathways to induce cell death in testicular tissue in adult male mice.

2.2. Objectives

2.2.1. Main Objective

To determine the effects of scrotal hyperthermia on the induction of the alkaliptosis and oxeiptosis molecular pathways that lead to testicular cell death in adult male mice.

2.2.2. Specific Objectives

- To determine the effect of scrotal hyperthermia on the genes involved in the molecular pathways of cell death related to oxeiptosis and alkaliptosis in the testicular tissue of adult mice.
- To determine the effect of scrotal hyperthermia on sperm analysis parameters, including total sperm count, motility, viability, and morphology in adult mice.
- To determine the effect of scrotal hyperthermia on testicular tissue by assessing the volume, number of testicular cells, and length and diameter of seminiferous tubules in adult mice.

2.2.3. Practical Objectives

The study of the mechanisms involved in testicular cell death after induction of scrotal hyperthermia can be used to more effectively asses the effects of different therapies and can be generalized to humans.

2.3. Hypotheses

- Scrotal hyperthermia increases the expression of genes involved in the oxeiptosis and alkaliptosis cell death pathways in adult mice.
- Scrotal hyperthermia reduces motility, viability, and the percentage of sperm with normal morphology in adult mice.
- Scrotal hyperthermia reduces the volume, the number of testicular cells, and the length and diameter of seminiferous tubules in the testicular tissue of adult mice.

3. Material and Methods

3.1. Acquisition and preparation of animals for experimentation

Twenty adult (8-10 weeks old) male NMRI mice with an average body weight of 26 g (range: 25 to 30 g) were purchased from the laboratory animal center at the Pasteur Institute of Iran, Tehran. The animals were kept in the Shahid Beheshti University Animal House in plastic group cages under controlled conditions (temperature around 20-23ºC, 12-hour light/dark cycles, and relative humidity of 50–65%). They were allowed 2 weeks of acclimation. The mice were fed pelleted food and had access to tap water ad libitum.

3.2. Grouping and the protocol for Testicular Hyperthermia

After the acclimation period, the animals were randomly divided into two groups: (I) control group (n = 10), which received no intervention, and (II) hyperthermia group (n = 10), in which the mice were exposed to testicular hyperthermia. The scrotal hyperthermia was performed according to the model introduced by Ziaeipour et al. For this purpose, the mice were first anesthetized with intraperitoneal injections of ketamine (100 mg/kg) and xylazine (5 mg/kg). Then, the lower third of the body, consisting of the scrotum, tail, and hind legs, was immersed in a water bath at 43°C for 20 minutes every other day for 5 weeks(11). Afterward, they were dried and returned to their cages. After the last testicular hyperthermia exposure, all mice were maintained for 35 days (the length of the sexual period of male mice) to allow for the second cycle of spermatogenesis. Subsequently, all animals were sacrificed for further evaluation.

3.3. Blood collection and Hormonal analysis

At the end of the 35-day interval and before sacrificing the animals, each mouse was anesthetized using a combination of ketamine (100 mg/kg) and xylazine (10 mg/kg), and blood was withdrawn from the heart using a standard 2.5 mL syringe. The blood in the syringe was then quickly transferred to a test tube without anticoagulant. The collected tubes were kept at 37°C for 15 minutes and then centrifuged at 5,000 rpm and 6,000 g for 10 minutes at 4°C. Serum was carefully separated with a pipette, transferred to a microtube, and stored at -70°C until hormone measurement. A commercial ELISA kit (IBL, Hamburg, Germany) was used to measure the level of testosterone. The measurements were reported in ng/mL(12,13).

3.4. Sperm Acquisition and Analysis

3.4.1. Sperm Sample Acquisition

After blood collection and while maintaining deep anesthesia, all mice were quickly decapitated. To obtain sperm samples, the entire ventral surface of the mice was sprayed with 70% alcohol. Using forceps and sterile scissors, the ventral area was opened, and after transecting the peritoneum and identifying the testicles, both testicles along with the epididymis were removed. The tail of the epididymis (which is white and located below the testicle) was separated from the surrounding fat tissue and transferred to a 60-mm Petri dish containing 1 mL of Ham's F-10 medium (HTF; Sigma Alderich, St. Louis, USA). It was then placed in an incubator for 15 minutes. Afterward, the tail of the epididymis was incised into smaller pieces with insulin needles and incubated at 5% CO_2 for 15 to 20 minutes at 37°C to release sperm into the medium. Next, 10 µL samples were taken from the medium, and each sperm mixture sample was transferred to a 1 mL microtube to evaluate sperm parameters(1,11,12).

3.4.2. Sperm Analyses

3.4.2.1. Total Sperm Count

To determine the total sperm count, 190 µL Ham's F-10 media was added to each microtube, and then well mixed. After sample uniformity, 10 µl of sperm suspension was poured on a warm (37°C) Neubauer hemocytometer slide (QC-LAB™, Nantong, China) and placed under phase contrast microscopy at 200X magnifications. In the end, the total sperm count was reported as cell per mL(14).

3.4.2.2. Total Sperm Count

To determine the extent of motility of sperm subjectively, the percentage of motile (progressive and non-progressive) and immotile sperm was determined in five fields of vision observed at 400X magnification(14).

3.4.2.3. Sperm Morphology

To study sperm morphology, 10 µL of sperm suspension was placed on slides, smeared, and stained using a commercial Diff-Quick staining kit (Ideh Varzan Farda Co., Tehran, Iran) that contains special stabilizers and dyes. These dyes penetrate the cell, resulting in the cytoplasm appearing pink-purple and the nucleus blue-purple (Fig. 3.1.). After the slides air dried, the number of sperm with normal morphology was expressed as a percentage, using immersion oil and a light microscope at 100X magnification(14).

3.4.2.4. Sperm Viability

To study sperm viability, sperm suspension and eosin-nigrosine dye (Merck™; Darmstadt, Germany) were combined in equal volumes (25 µL each), and one drop of the mixture was placed on a lubricated slide. After the smear dried at room temperature, a total of five fields were examined with immersion oil and a light microscope (Nikon, Tokyo, Japan) at 100X magnification(14). Using this staining method, the contrast between the cells and the background was enhanced by using the nigrosine dye, which acts as a negative stain and is not absorbed by the cells. Eosin dye readily permeates the damaged membrane of dead sperm, giving the appearance of pink sperm. Live sperm cells, on the other hand, have a healthy, undamaged membrane that prevents the dye from penetrating readily, giving the appearance of white sperm.

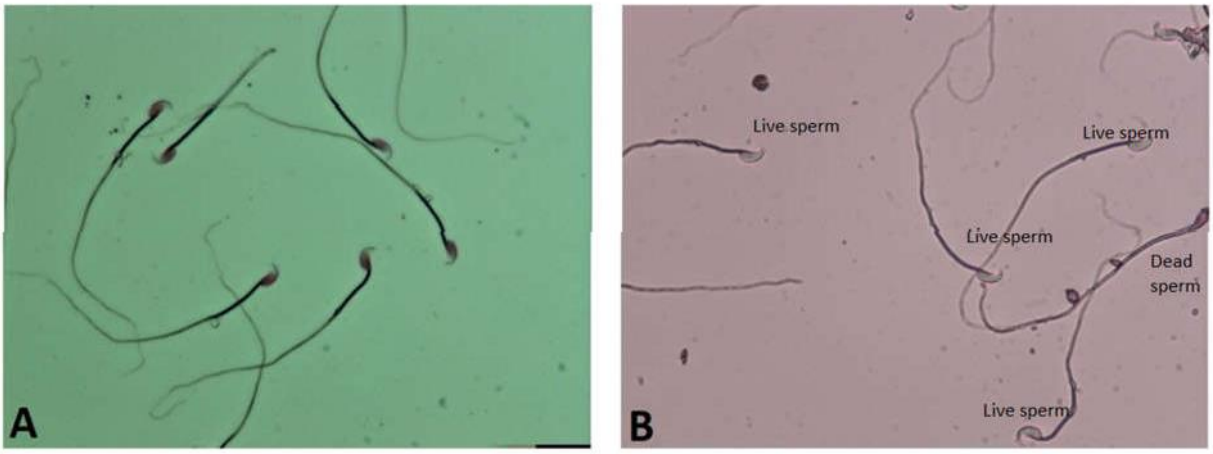

Figure 3.1. Images of sperm stained with (A) Diff Quick and (B) Eosin-Nigrosine.

3.5. Testicular tissue acquisition and histopathological analysis

3.5.1. Tissue Acquisition and preparation

After the extraction of the testicles from the body, they were weighed using a digital weighing device. The left testis was designated for biochemical and genetic studies, while the right testis was used for histological and stereological studies. The right testis was submerged in 4% paraformaldehyde for 48 hours. After that, it was embedded in paraffin blocks. Using a rotary microtome (Leica RM2125 RTS, Germany), serial sections of 5 µm and 20 µm thickness were made: 5 µm sections for and seminiferous tubule diameter, and 20 µm sections for estimating overall testicular volume and numerical density of testicular cells. All sections were stained with Hematoxylin and Eosin (H&E) (Sigma Aldrich, St. Louis, USA)(11–13,15).

3.5.2. Histological and stereological analyses

3.5.2.1. Estimation of the testicular volume

Ten sections of 20 µm thickness were selected using systematic uniform random sampling and were used for the estimation of testicular volume. The live image of each testicular section was evaluated using a projection microscope (Olympus, Tokyo, Japan) at a final magnification of 25X. A dot matrix was superimposed on the images using stereological software developed at the Stereology Research Center (Shahid Beheshti University of Medical Sciences). The volumes were calculated using the Cavalieri method, whereby the overall volume of the testis was determined using the point counting method as the product of the areas and the distances between the sampled intervals(15–17). The volume of the testicles(v) was estimated by following formula(15,16)

$$V = \sum P \times \frac{a}{p} \times d,$$

ΣP: The total number of points counted that intersected the testicular sections.

a/p (area per point): area allocated to each point divided by the magnification.

d: Distance between sampled sections.

3.5.2.2. Determination of numerical density and total number of testicular cells

Ten randomLy selected 20 µm sections were used to estimate the numerical density of testicular cells. The live image of each section was evaluated using a projection microscope (Olympus, Tokyo, Japan) at a final magnification of 100X. The position of the microscopic fields was chosen by systematic uniform random sampling, moving the table in x- and y-directions at equal intervals. The optical dissector technique was used to estimate the numerical density of cells in the testes(15,16,18). The testicular cell and germinal cells were distinguished from a morphological point of view and counted separately. Leydig cells, which are polyhedral in shape and have spherical nuclei with eosinophilic cytoplasm, are located in the interstitial tissue of the seminiferous tubules. Sertoli cells, situated at the base of the epithelium of the tubules, have large, basal, oval, pale, invaginated nuclei with a prominent nucleolus. Spermatogonia, positioned at the base of the germinal epithelium, have either dark or light-colored round nuclei and are dome-shaped cells. Primary spermatocytes, the largest cells of the seminiferous epithelium, are located in the middle of the germinal epithelium. The round spermatids consist of spherical cells that are oriented toward the lumen (Figure 3.2)

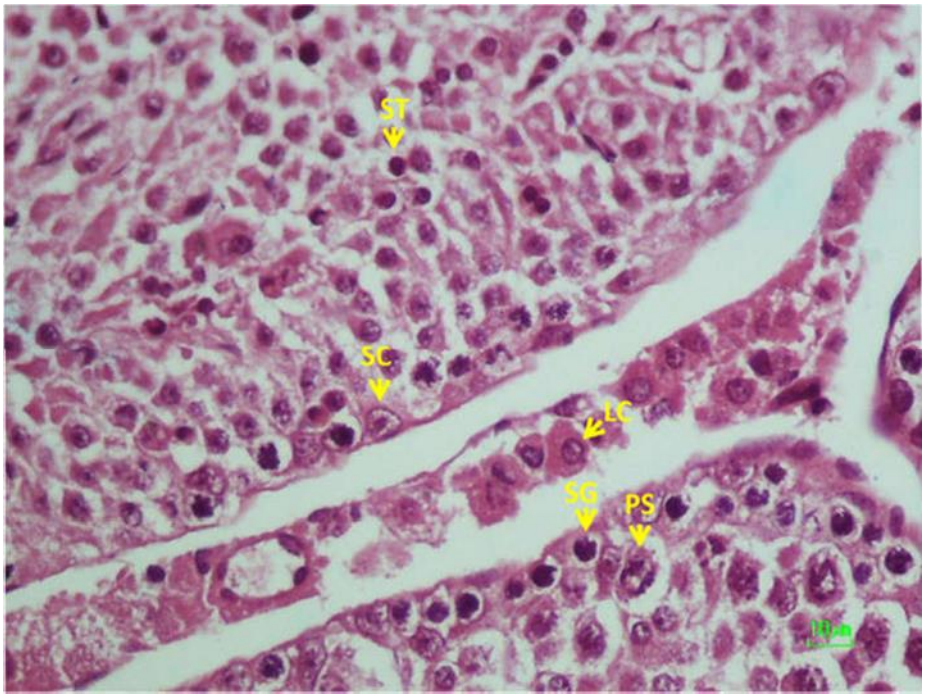

Figure 3.2. Photomicrograph of the sample of testis stained with H&E, 100X, Showing testicular cells and germinal cells: Leydig cell (LC), Spermatogonia (SG), Primary spermatocyte (PS), Spermatid cell (SC).

An unbiased counting frame probe (designed at the Stereology Research Center of Shahid Beheshti University of Medical Sciences) with counting areas of 35 × 35 μm², featuring inclusion and exclusion lines, was used, And superimposed on the live images displayed on the monitor. The frame lines help avoid the edge effect and biased cell counting. A cell was counted if it fell completely within or partially on the inclusion line, while not touching the exclusion line. The top and bottom of each tissue section, each 2 μm thick, were excluded from counting by the dissector to avoid cutting artifacts that appear on the upper and lower surfaces of the tissue sections. Thus, the height of the dissector for each section was determined to be 16 μm. The actual thickness of tissue in each section was measured by accurately determining the focal position of the microscope stage along the z-axis using a microcater (Heidenhain, Traunreut, Germany) attached to the microscope stage for each microscopic field, and then averaged. The numerical density (NV) of each cell type was estimated using the following formula(15,16):

$$N_v = \frac{\sum Q}{\sum F \times h \times \frac{a}{f}} \times \frac{t}{BA}$$

ΣQ: Total number of cells that were counted.

ΣF: Total number of unbiased counting frames in all fields.

h: height of the dissector (here was 16 µm).

a/f (area per frame) the ratio of the area of the probe to the magnification (35×35 μm^2 / 100).

t: actual thickness of the tissue section.

BA: the block advance of the microtome set on 20 µm.

The total number of the cells was estimated by multiplying the numerical density (Nv) by the V (testis).

3.5.2.3. Determination of the length of seminiferous tubules

Ten sections of 5 µm thickness were selected using systematic uniform random sampling to estimate the length of the seminiferous tubules. Five random fields were chosen from each section using a projection microscope at 10X magnification. The live image of each field was evaluated using a projection microscope (Olympus, Tokyo, Japan) at a final magnification of 100X. The number of seminiferous tubules was estimated by overlaying an unbiased counting frame (designed at the Stereology Research Center of Shahid Beheshti University of Medical Sciences) with a counting area of 625 µm × 625 μm^2 randomLy on the monitor. Tubules with their profiles completely within the counting frame were counted. The length density (L_v) of the seminiferous tubules was estimated using the following formula(15,16):

$$L_v = \frac{2\sum Q}{\sum F \times \frac{a}{f}}$$

ΣQ: Total number of the tubule's profiles counted.

ΣF: Total number of unbiased counting frames in all fields

a/f (area per frame) (625 µm × 625 μm^2 /100)

To calculate the absolute length of the seminiferous tubules, the length density (Lv) was multiplied by the total volume of the testis.

3.6. RNA extraction and gene expression analysis

3.6.1. RNA Extraction and Preparation

3.6.1.1. RNA Extraction

RNA extraction from testis tissues was performed in a fully sterile environment with no contamination. All extraction steps were performed at 4°C and on ice. All other tubes and

consumables, including aluminum plates and sample tips, were also autoclaved. RNA extraction was performed under the RNA extraction hood.

Materials required for RNA extraction:

- RNA Extraction kit (Total RNA Extraction Kit) (Jena Bioscience, Jena, Germany)
- Chloroform (Merck™, Darmstadt, Germany)
- Isopropanol (Merck™, Darmstadt, Germany)
- Ethanol (Merck™, Darmstadt, Germany)
- DEPC-treated Water (RNase free) (Jena Bioscience, Jena, Germany)

Equipment required for RNA extraction:

- Refrigerated Centrifuge (Eppendorf, Hamburg, Germany)
- Vortex (Eppendorf, Hamburg, Germany)
- Sampler (Gilson, Middleton, USA)
- RNase free Micro tube and pipette tips (Eppendorf, Hamburg, Germany)
- Sterile aluminum sheets
- Surgical blade (Bistoury) (QC-LAB™, China)

The extraction steps were as follows:

1. First, the frozen tissue was digested on the aluminum foil using the sterile surgical blade.

2. The digested tissue was transferred to a 1.5 mL tube and 1 mL of lysis buffer was added to it, and then the tube was vortexed to achieve a homogeneous suspension.

3. 200 µL chloroform was added to the suspension and thoroughly mixed thoroughly by inverting the tube for 15 seconds.

4. The mixture was placed on ice for 5 minutes.

5. The tube was placed in a refrigerated centrifuge for at 4°C and 12,000 rpm for 15 minutes.

6. At this point the tube contained 3 phases which could be seen from the top as a colorless phase, a white intermediate phase and a lower green phase where the RNA was in the upper

colorless phase which was carefully separated by a sampler into a Transfer to another sterile tube.

7. Isopropanol was added while removing the same volume of solution and the tube was shaken several times and incubated for 10 minutes at -20°C and then for 10 minutes in a refrigerated centrifuge at 4°C at 12000 rpm.

8. The supernatant was decanted and 1 mL of 80% ethanol was added to the tube and then centrifuged again for 5 minutes.

9. The supernatant was removed and the tube was dried, then the precipitated RNA was dissolved in DEPC-treated water, and then the tube was transferred to a -70°C freezer.

Qualitative evaluation of extracted RNA

To evaluate the quality of the extracted RNA, 2 µL of RNA was applied to a 2% agarose gel. Optimal quality of RNA was generated on the clear 2-band gel corresponding to 18s and 28s ribosomal RNAs, and other RNAs in the sample were identified as smear. This procedure ensured the quality of the extracted RNA.

Quantitative assessment of extracted RNA

A Nanodrop™ 2000/2000C device (Thermo Fisher Scientific™, Waltham, USA) was used to assess the amount of RNA extracted. After diluting the RNA in distilled water, its absorbance at 260 nm was measured. Additionally, to evaluate the quality of the RNA and verify the absence of contamination with protein and DNA, the absorbance ratio of 260 to 280 was examined. A value between 1.6 and 1.9 indicates optimal RNA quality.

3.6.1.3. Removal of DNA contamination from extracted RNA with DNase

To remove DNA contamination from the RNA samples, they were treated with a commercial DNase I (RNase-free) kit (Thermo Fisher Scientific™, Waltham, USA)(Tab. 3.6.1.3) according to the manufacturer's protocol. First, 10 µL of the RNA sample, 1 µL (1 U) of DNase I, and 1 µL of reaction buffer with $MgCl_2$ (10X) were added to an RNase-free microtube (Eppendorf, Hamburg, Germany) and mixed. The mixture was then incubated at 37°C for 10 minutes. After that, 1 µL of 50 mM EDTA was added to the microtube, and it was incubated again at 65°C for 10 minutes.

Table 3.6.1.3. Contents of the DNase I kit

Components	Quantity
DNase I, RNase-free (1 U/µL)	**1mL**
Reaction buffer with MgCl2(10X)	**1mL**
EDTA (50 mM)	**1mL**

3.6.2. cDNA Synthesis

The transition from RNA to cDNA is necessary for RT-PCR and real-time PCR reactions and is accomplished using random hexamer and oligo dT primers along with reverse transcriptase enzymes. Oligo-dT primers are designed to bind to the poly-A tail, but some RNAs do not have this feature. Since certain RNAs lack a poly-A tail, the use of random hexamer primers to amplify these types of RNA is of great importance. The commercial PrimeScript™ RT Reagent Kit (Takara, Shiga, Japan) (Tab.3.6.2.1) was utilized for cDNA synthesis in this project. The cDNA synthesis steps were performed in a suitable hood on ice, using sterilized and autoclaved equipment.

Table 3.6.2.1. cDNA Synthesis kit ingredients

Components	Quantity
5 X PrimeScript™ Buffer (for Real Time)	**400 µL**
PrimeScript™ RT Enzyme Mix I	**100 µL**
Oligo dT Primer (50µM)	**100 µL**
Random 6-mers (100µM)	**100 µL**
RNase Free dH2O	**1mL**

According to the Tab. 3.6.2.2, the mixture for removing DNA contamination was prepared. The reaction microtube was placed inside the Thermal Cycler TC-1000S (Dlab Scientific Co., Beijing, China) with the following program: 15 minutes at 37°C for three cycles, followed by 5 seconds at 85°C. After this, the mixture tube was placed on ice (4°C).

Table 3.6.2.2. The amount of consumable required for cDNA Synthesis

Components	Final concentration	Quantity
5 X PrimeScript™ Buffer	1X	**2 µL**
PrimeScript™ RT Enzyme Mix I	-	**0.5 µL**
Oligo dT Primer (50 µM)	25 pmol	**0.5 µL**
Random 6-mers (100 µM)	50 pmol	**0.5 µL**
Total RNA	Up to 500 ng	**1 µL**
RNase Free dH2O		**6.5 µL, Total Volume 10 µL**

cDNA quality evaluation by RT-PCR reaction

To assess the quality of the synthesized cDNA, an RT-PCR reaction was performed using the Taq DNA Polymerase 2x Master Mix Red Kit (Ampliqon, Odense, Denmark) according to the Tab. 3.6.2.3. The synthesized cDNA was amplified for 35 cycles using PCR Master Mix (Sigma Aldrich, St. Louis, USA). The PCR product was then electrophoresed on a 2% agarose gel (Iranroyan.co, Tehran, Iran) and visualized using ethidium bromide staining (Thermo Fisher Scientific™, Waltham, USA).

Table 3.6.2.3. The amount of consumable required for the RT-PCR reaction

Components	concentration	Quantity
cDNA	-	**2 µL**
Taq DNA Polymerase Master Mix Red	2x	**10 µL**
KEAP1 Forward Primer	10 pmol /µL	**1 µL**
KEAP1 Reverse Primer	10 pmol /µL	**1 µL**
Distilled Water		**6 µL,Total Volume 20 µL**

Quantitative evaluation of target genes with Real-time PCR

Real-time PCR, which is similar to RT-PCR except that electrophoresis is not required to monitor the PCR product, was used to quantify gene expression. This gene expression quantification method has a very high sensitivity and can be performed in a short time, and the amplification of the product from the same initial cycles can be observed by emitting a fluorescence beam and receiving it by the device. This fluorescence beam is generated by the reporter molecule, either in the form of sequence-specific identifiers such as TaqMan probes or in the form of dyes that bind to double-stranded DNA such as SYBR Green. In this study, SYBR Green I (Sinaclon, Tehran, Iran) dye was used, which produces a small fluorescence beam when free. But after being placed in the small groove of the double-stranded DNA molecule, the amount of this beam increases more than 1000 times. This dye's binding to non-specific DNA means that it can bind to any double-stranded DNA, including primer dimers and non-specific amplified products. To control this phenomenon and verify the accuracy of the reaction results, a melting curve was added to the program at the end of the real-time PCR reaction, and the products were loaded onto an agarose gel to verify that there was no non-specific binding or dimer. The program of the melting curve was such that at the end of the reaction the temperature rose continuously by 0.5°C from 70°C to 95°C. At a certain temperature, PCR products produce a peak in the curve called the product Tm ([Primer] melting temperature). At this temperature, 50% of the double-stranded DNA of the denatured product is reduced, reducing the emitted fluorescence Tm. PCR products vary by product length and GC percentage in the sequence.

3.6.3. Primer Design and Real Time PCR

Using the NCBI site and after inserting the sequence of the genes under study, primers were designed for the target genes, including the MUS genes: ikbkb-nfκb-ca9, keap1, pgam5 and aifm1 and the mouse housekeeping gene, β-actin, and using the primer blast option, the primers were checked for binding to other points in the genome.

The following list (Tab. 3.6.3.1) should be considered when designing suitable primers for the real-time PCR reaction:

- It is better for primers to produce products with a length of 150-220 bp, since products smaller than this value cannot be derived from the primer dimer, and products larger than this complicates the reaction.
- Primers should be between 18 and 24 nucleotides in length to prevent formation of homodimers and heterodimers.
- The GC percentage of the primers should be between 45% - 65% and their Tm value should be in the range of 55% - 65%, and the primers should be designed to allow the formation of secondary structures and complementary hybridization in the 3' end region impede.

Table 3.6.3.1. Primers sequences and corresponding product sizes

Gene	Sequence 5′→3	PCR product
NF-κB	F: GAAGGAGATCATCCGCCAGG	165 bp
	R: GCATTCGGGGCTTTGCTATC	
IKBKB	F: CAGGCACCGTTCACACATAC	184 bp
	R: AGGCCCTCGTTTGTCTTGC	
CA9	F: TGTTCTGCCCAGTGAAGAGGA	211 bp
	R: CCAGAGTAGGGTGCCTCCATAG	
KEAP1	F: AGCAGCGTGGAGAGATATGAG	143 bp
	R: TTAAGCCGGTTAGTCCCGTC	
PGAM5	F: AGAAGACGAGTTGACATCCAG	142 bp
	R: AGCCTGTTCCCGACCTAATG	
AIFM1	F: CGAAGGCGAGTAGAGCATCA	121 bp
	R: CAGGACCCAAATCACTCCAGAA	
ACTB	F: GATCTCCTTCTGCATCCTGT	191 bp
	R: TGGGCATCCACGAAACTAC	

Real-time PCR reaction conditions

In this study, the SYBR Premix Ex Taq II kit (Takara, Shiga, Japan) was used, which contains a ready-made master mix and includes all materials required for the reaction except primers and cDNA. The number of reaction cycles can vary between 40 and 50. In this project, 40 cycles were

performed in the LineGene 9600 real time PCR machine (Bioer, Hangzhou, China). The amount of material used for a 20-microliter tube was as Tab. 3.6.3.2

Table 3.6.3.2. Real-time temperature PCR program

Process	Temperature °C	Time	Number of Cycles
Hold	95	10'	**1**
Denaturation	95	15"	**40**
Annealing & Extension	72	20"	**40**
Melting Curve analysis	70-95	Rising by 0.5°C	**1**

Determining PCR product specificity

Determination of PCR product specificity by melting curve analysis

Melting curve analysis was performed to separate the desired specific product from other non-specific products and primers. In the double-stranded state of the DNA, a fluorescent dye attaches to it and emits a strong signal. As the temperature increases, the DNA is denatured and the fluorescence signal decreases until, at the Tm point, half of the product is completely denatured and the fluorescence signal suddenly decreases, giving rise to a peak in the curved diagram. Each product has its own Tm, creating unique peaks.

Determination of PCR product specificity by electrophoresis on agarose gel

The products were electrophoresed on 2% agarose gel to check the size of the products and the absence of primer-dimer. If non-specific bands are seen on the agarose gel, these bands can be removed by changing the PCR reaction parameters. For example, reducing the amount of reaction primers can remove the observed band in the primer dimer region, or non-specific bands that are long product length can be removed by reducing the time of the extension phase or increasing the temperature of this phase.

3.7. Data analysis

All of the dependent variables were quantitative, and the only qualitative variable was the presence or absence of scrotal hyperthermia, which was used for grouping. Thus, no summary statistics were needed for the qualitative variable, while the mean (± SD) was used for summary statistics of the quantitative data. The Kolmogorov-Smirnov test was used to determine the normality of the data. For normally distributed data, an independent samples t-test was used, and

for non-normally distributed data, the Mann-Whitney test was used. A *P*-value of < 0.05 was considered statistically significant. LinRegPCR (version 10.1) and REST (version 2008) software were used to analyze real-time PCR data. For other data, statistical analysis was performed using GraphPad Prism software (version 9.3.1).

3.8. Ethical principles of research

This study was conducted under the Procedure for Working with Laboratory Animals published by the Ministry of Health, Treatment and Medical Education of Iran. (IR.SBMU.MSP.REC.). The principles to be observed are: The size of the cage and the number of mice were such that the animals could rest, move and live in it. The material used to make the cage is clear plastic that can be seen from the inside of the wall inside the cage. The cage was designed in such a way that they could not escape and were not injured. Mice were not kept with their predators. Mice have always had free access to water and healthy food. A stable and pleasant temperature, the right light/dark alternation and air circulation were always taken care of. The carcasses of the killed mice were far from the mice's nests and they could not smell the dead animal. The animal cage was kept clean every few days by changing the straw and the smell of garbage didn't bother them. Sick mice were not included in the study at all. The mice were given time to become familiar with the laboratory, the laboratory tools, and the researcher. Prior to the study, the minimum number of animals required to obtain statistical data was estimated. Prior to the study, it was clear that there was no better alternative than using mice in this study. Efforts were made in this study to reduce harm to animals.

4. Results

4.1. Sperm parameters

Our results showed that sperm were absent in the hyperthermia group. All mice subjected to scrotal hyperthermia exhibited clinical signs of azoospermia and oligospermia after the induction of hyperthermia. In this study, the total sperm count in the hyperthermia group differed significantly from that in the control group ($P < 0.001$). Additionally, sperm motility in the hyperthermia group was statistically significantly different from that in the control group ($P<0.001$). Sperm viability in the hyperthermia group was also statistically significantly different from the control group ($P<0.001$). Based on our results, normal sperm morphology in the hyperthermia group differed significantly from that in the control group ($P<0.001$) (Fig. 4.1).

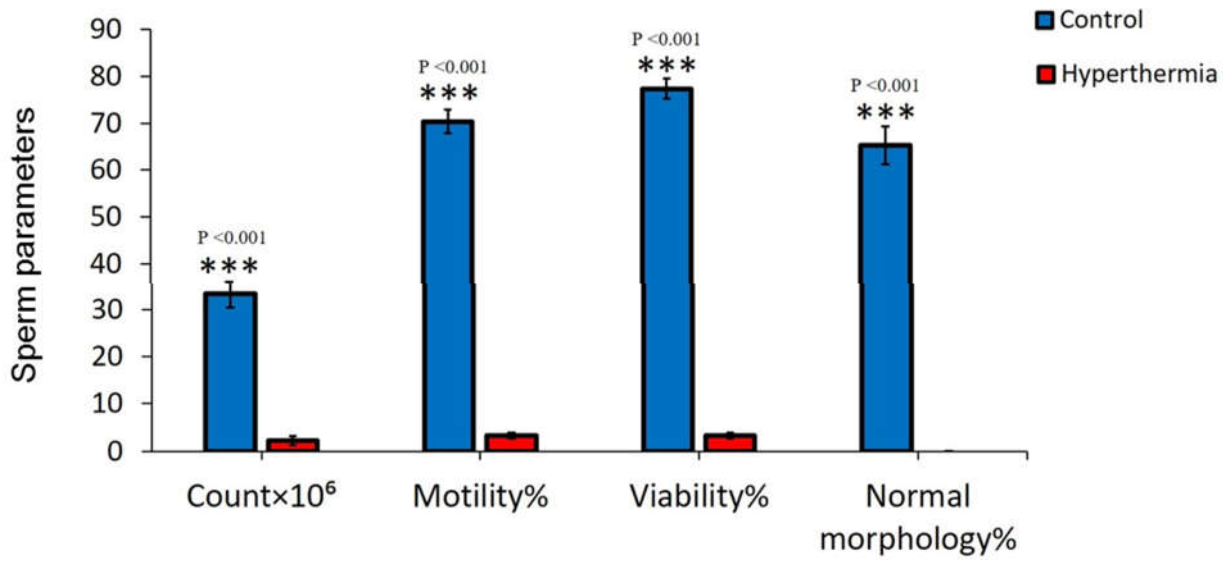

Figure 4.1. Total sperm count, percent of sperm motility, percentage of sperm survival and percent of normal morphology of testis in different groups (***$P<0.001$). Data represent as Mean ± SD.

4.2. Serum testosterone

Measurement of serum testosterone showed a significantly lower concentration in the hyperthermia group than in the control group (*P*<0.001).

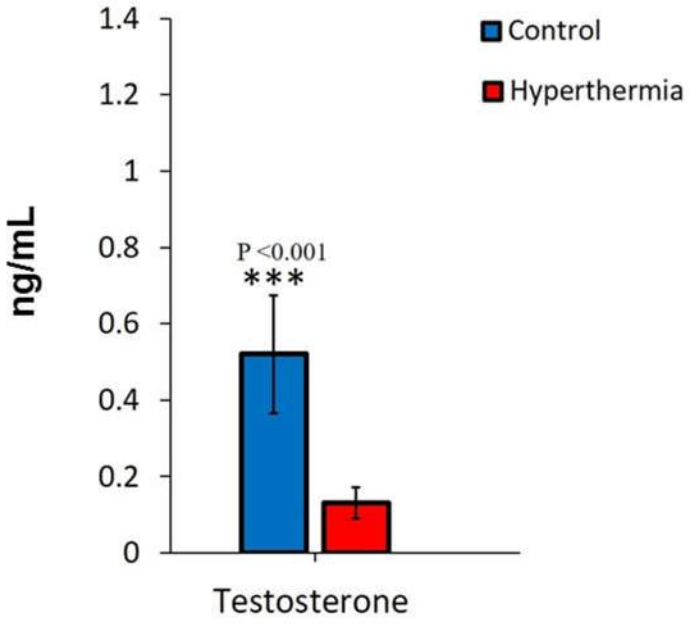

Figure 4.2. Serum testosterone in hyperthermia group compared with control group. Data represent as Mean ± SD.

4.3. Histopathological and Stereological analysis

Testis weight was significantly lower in hyperthermia group compared to the control group (*P*<0.001). Testicular volume was also significantly less in the hyperthermia group than in the control group (*P*<0.001). At the cellular level, a significant reduction in the total number of spermatogonia, primary spermatocytes, and spermatids was observed in the hyperthermia group compared to the control group (*P*<0.001 for all). Stereological results showed that the numbers of Sertoli and Leydig cells were significantly lower in the hyperthermia group compared to the control group (*P*<0.001 for both) (Fig. 4.3). The length of the seminiferous tubules was significantly lower in the hyperthermia group compared to the control group (*P*<0.001) (Fig. 4.4).

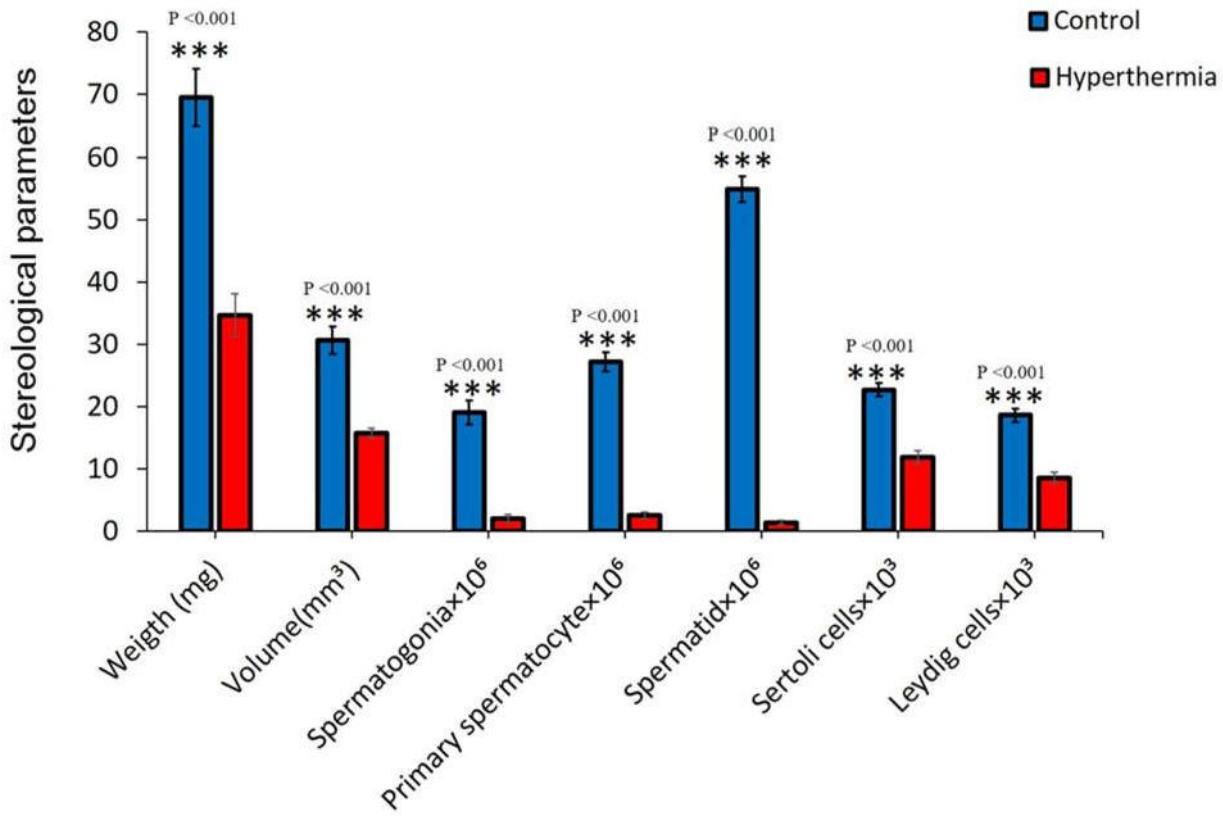

Figure 4.3. Testis weight, testis volume, number of spermatogonia, primary spermatocytes, round spermatids, Sertoli cells and Leydig cells of testes in different groups (***P*<0.01). Data represent as Mean ± SD.

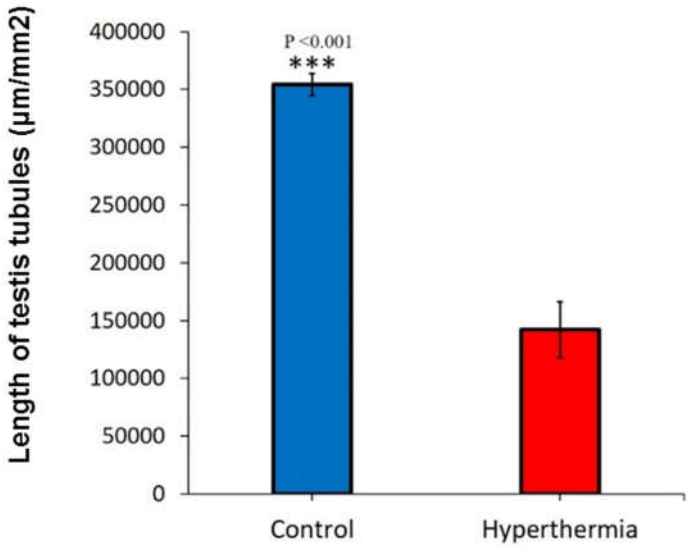

Figure 4.4. (A) Seminiferous tubule length in different groups (***P<0.001). Data represent as Mean ± SD.

4.4. Real-time PCR analysis

4.4.1. Alkaliptosis Pathway gene expressions

Real-time PCR analysis

As shown in Figure 4.5, the relative expression, based on the expression ratio of a target gene versus a reference gene of *NF-κB* was significantly increased (3.32 ± 1.12 ,P<0.001), while the relative expression of CA9 exhibited a significant decrease(0.51 ± 0.08, P<0.0001).

For the IKBKB gene, the relative expression showed no significant difference between scrotal hyperthermia and control groups. In general, these results indicate an alteration in the expression of alkaliptosis genes, leading to impaired spermatogenesis after testicular hyperthermia.

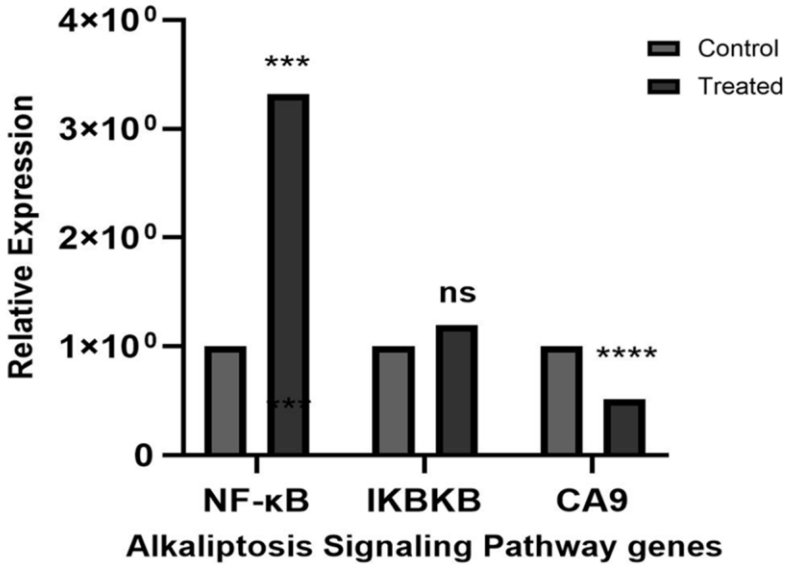

Figure 4.5. Relative expressions level of NF-κB, IKBKB and CA9 genes in scrotal hyperthermia group compared to the control group (****P*<0.001, *****P*<0.0001 and *ns*= non-significant).

Melting curve analysis of NF-κB, IKBKB and CA9 genes detected by realtime PCR. cDNA samples are amplified in real-time PCR with specific set of primers and melting curve analysis is performed to confirm the identity of the PCR products. Amplification plot, the increase in fluorescence signal as the PCR cycles progress,and melting curves of NF-κB, IKBKB and CA9 genes are shown in the Figs:4.6-4.11.

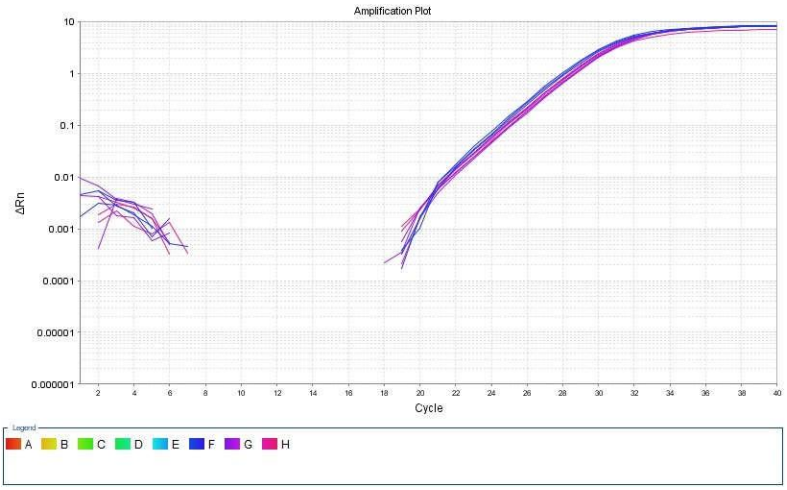

Figure 4.6: Amplification plot of IKBKB gene detected by real-time PCR. PCR cycles (X axis) were plotted against fluorescence intensity (Y axis).

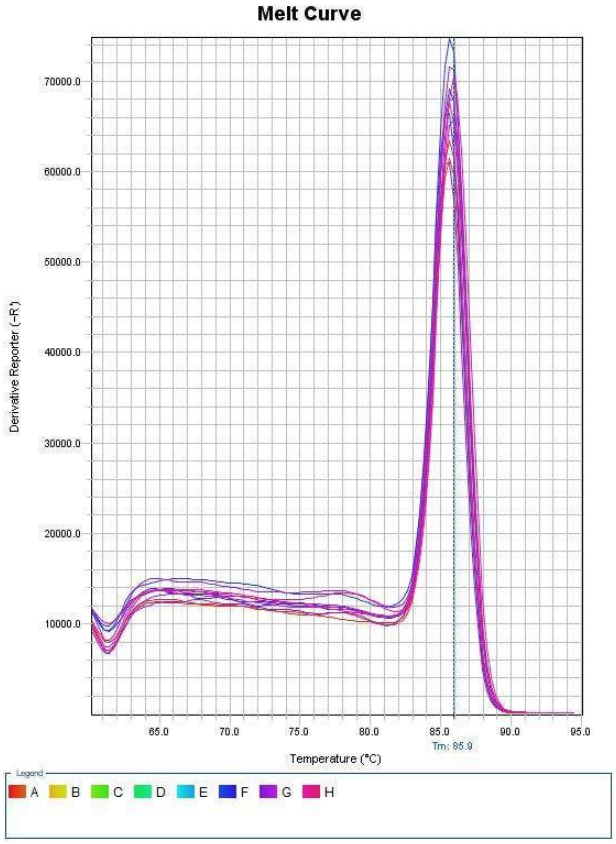

Figure 4.7: Melt curve of IKBKB gene detected using real-time PCR. The figure shows a melting temperature (Tm) of IKBKB PCR products as 85.9°C with no amplifications detected in negative controls.

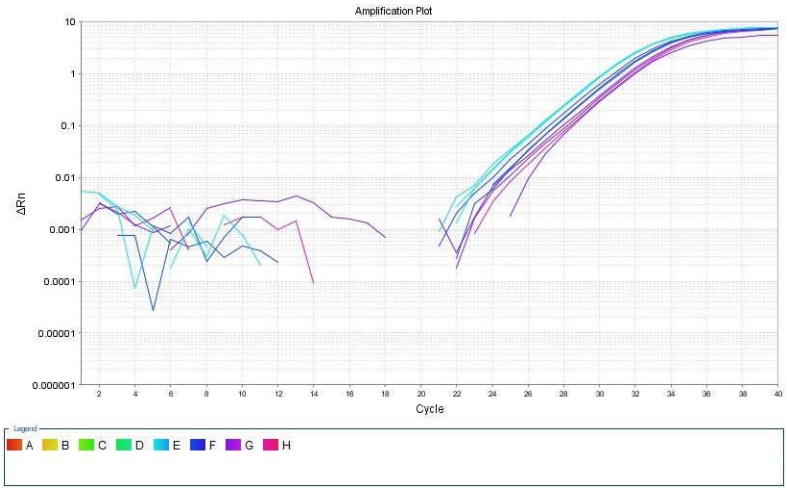

Figure 4. 8: Amplification plot of NF-κB gene detected by real-time PCR. PCR cycles (X axis) were plotted against fluorescence intensity (Y axis).

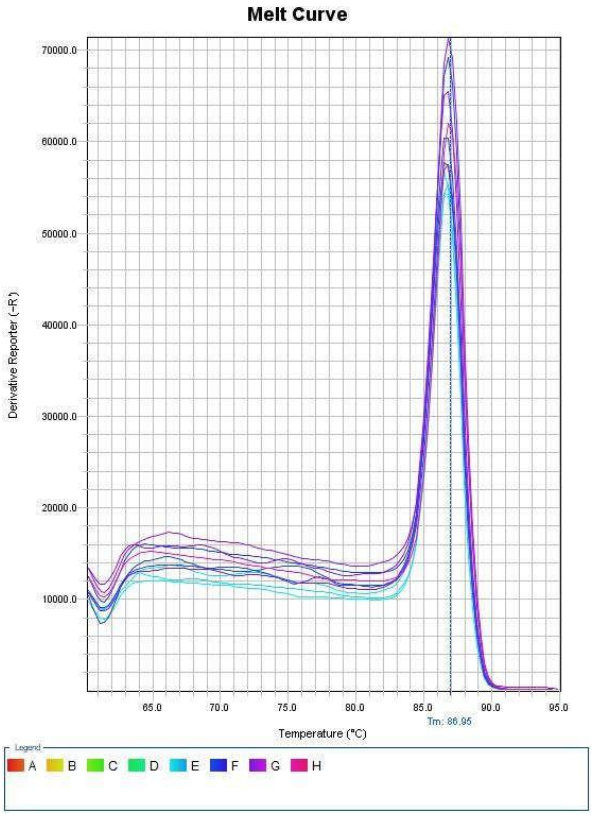

Figure 4. 9: Melt curve of NF-κB gene detected using real-time PCR. The figure shows a melting temperature of NF-κB PCR products as 86.95°C with no amplifications detected in negative controls.

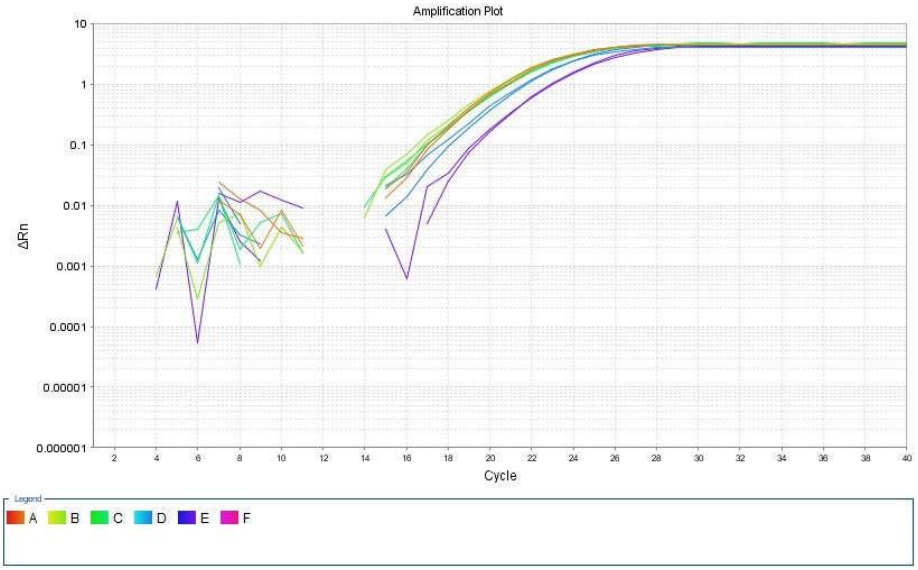

Figure 4.10: Amplification plot of CA9 gene detected by real-time PCR. PCR cycles (X axis) were plotted against fluorescence intensity (Y axis).

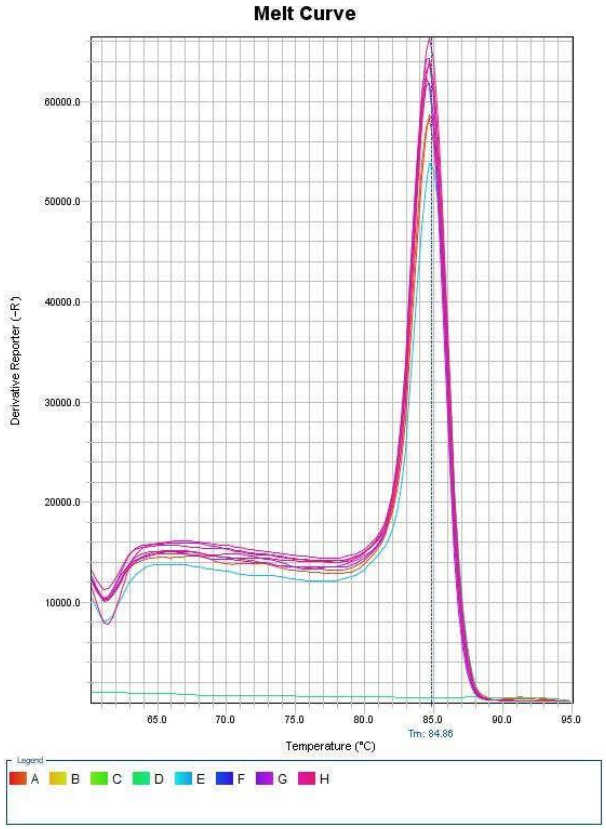

Figure 4.11: Melt curve of CA9 gene detected using real-time PCR. The figure shows a melting temperature of CA9 gene as 84.86°C with no amplifications detected in negative controls.

4.4.2. Oxeiptosis Pathway gene expressions

Considering the genes involved in oxeiptosis pathway, the relative expression of the AIFM1 gene was decreased significantly (0.23±0.05, *P*<0.001) in the scrotal hyperthermia group compared to the control group. Also, KEAP1 and PGAM5 genes demonstrated a significant increase (5.16± 1.03, *P*<0.001 and 2.50±0.21, *P*<0.0001) in the scrotal hyperthermia group compared to the control. (Fig. 4.12).

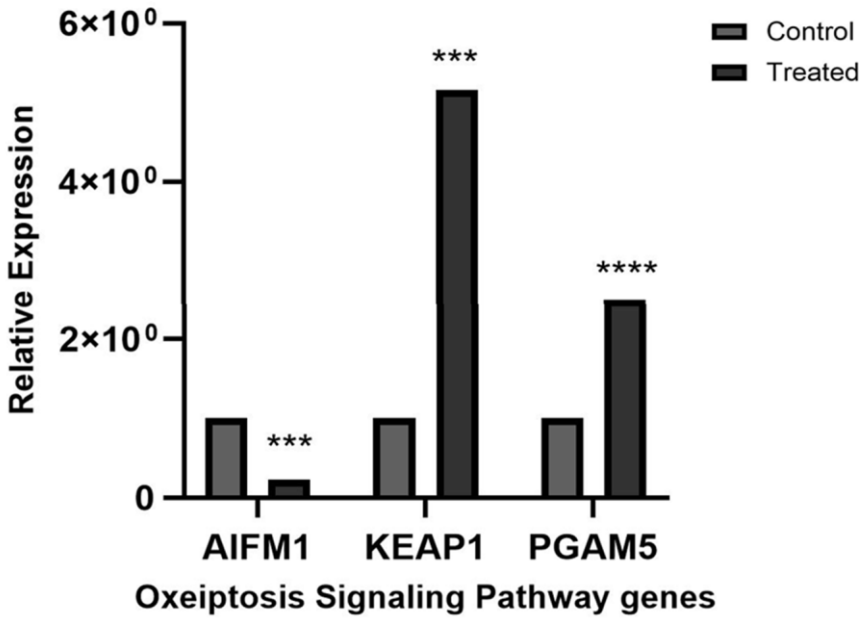

Figure 4.12. Relative expressions of AIFM1, KEAP1 and PGAM5 in scrotal hyperthermia group compared to the control group, (****P*<0.001 and *****P*<0.0001). Data normalized to the expression of the housekeeping gene, β-actin.

Amplification plots and melting curves of AIFM1, KEAP1 and PGAM5 genes are shown in Figs. 4.13-4.18.

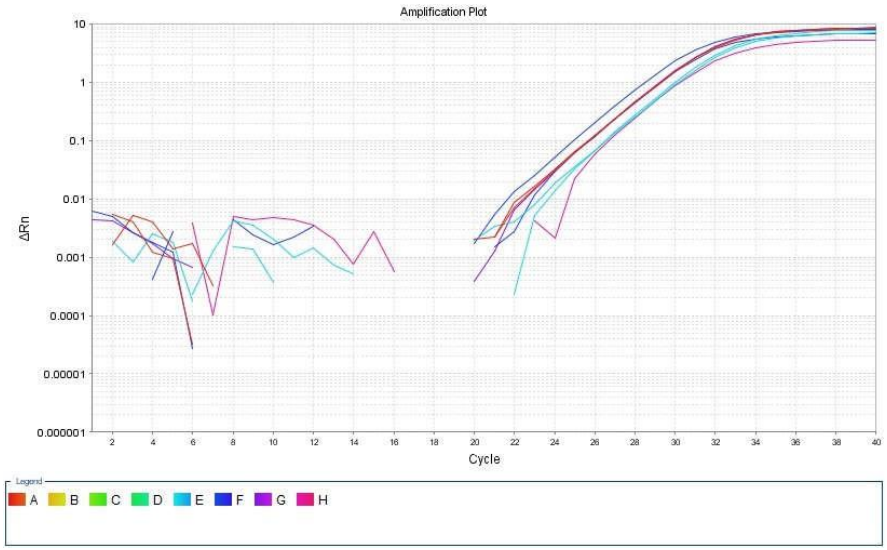

Figure 4.13: Amplification plot of AIFM1 gene detected by real-time PCR. PCR cycles (X axis) were plotted against fluorescence intensity (Y axis).

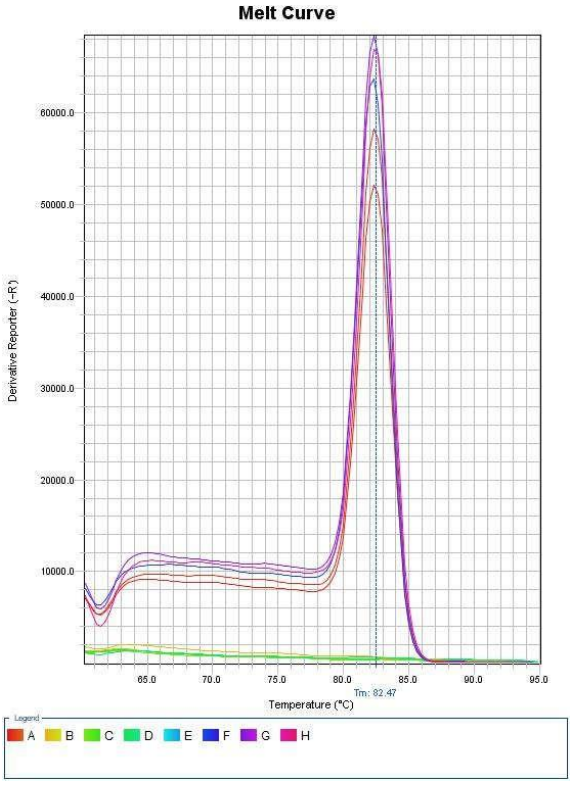

Figure 4.14: Melt curve of AIFM1 gene detected using real-time PCR. The figure shows a melting temperature of AIFM1 gene as 82.47°C with no amplifications detected in negative controls.

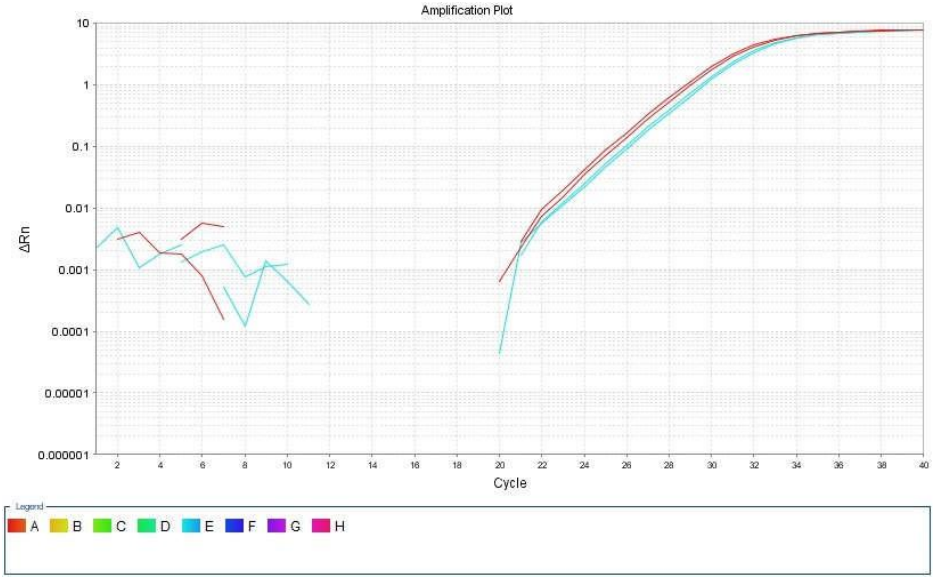

Figure 4.15: Amplification plot of PGAM5 gene detected by real-time PCR. PCR cycles (X axis) were plotted against fluorescence intensity (Y axis).

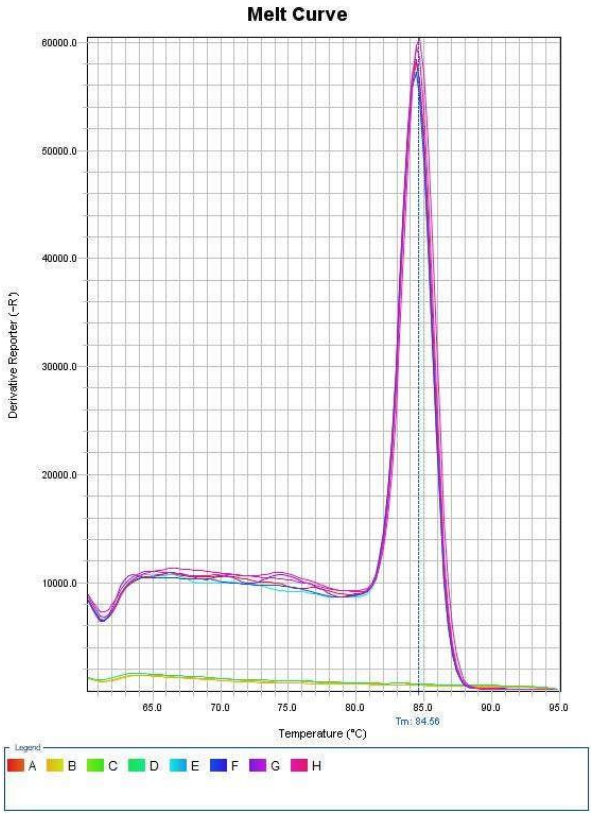

Figure 4.16: Melt curve of PGAM5 gene detected using real-time PCR. The figure shows a melting temperature of PGAM5 gene as 84.56°C with no amplifications detected in negative controls.

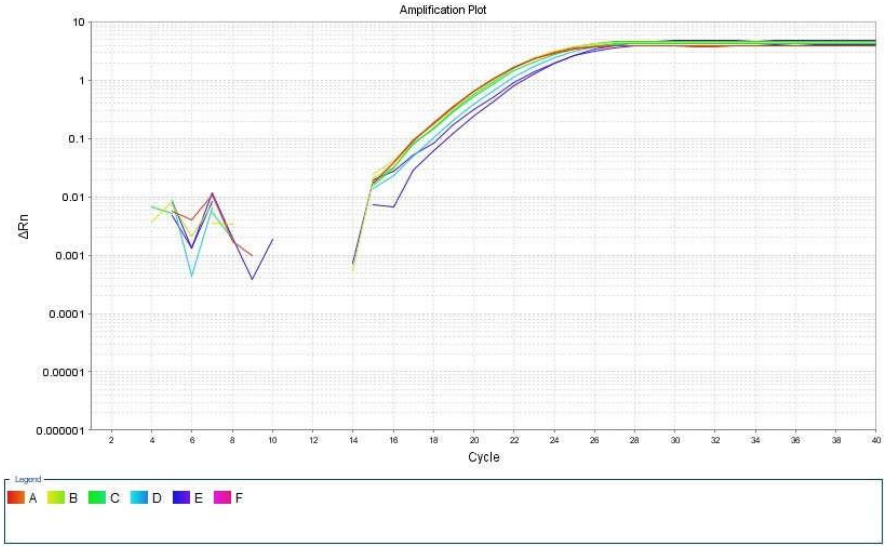

Figure 4.17: Amplification plot of KEAP1 gene detected by real-time PCR. PCR cycles (X axis) were plotted against fluorescence intensity (Y axis).

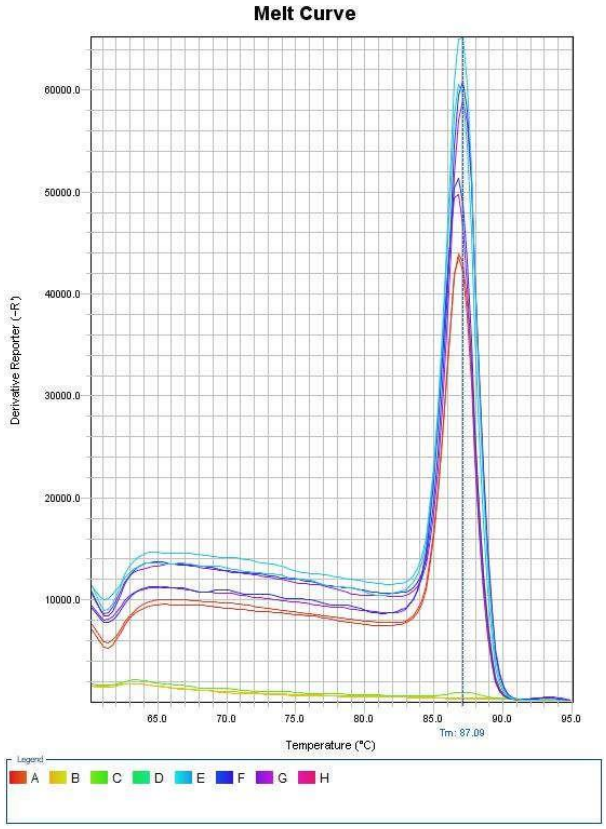

Figure 4.18: Melt curve of KEAP1 gene detected using real-time PCR. The figure shows a melting temperature of KEAP1 gene as 87.09°C with no amplifications detected in negative controls.

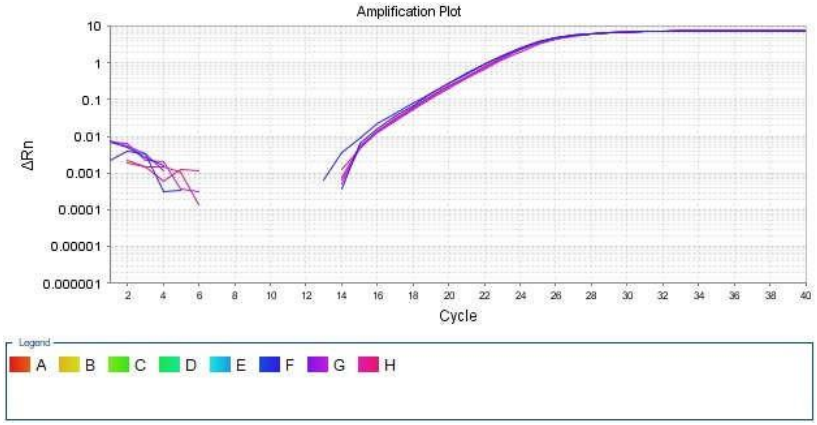

Figure 4.19: Amplification plot of β-actin gene detected by real-time PCR. PCR cycles (X axis) were plotted against fluorescence intensity (Y axis).

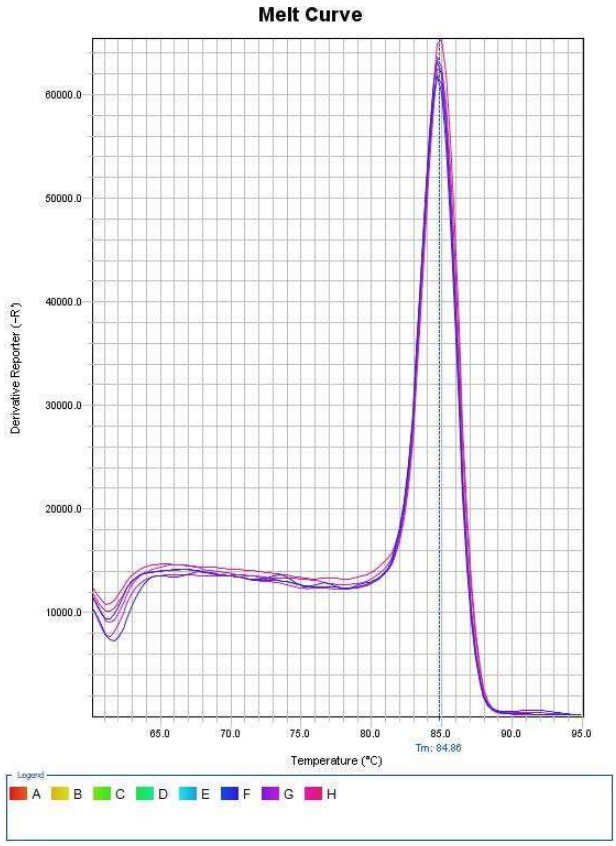

Figure 4.20. Melt curve of β-actin gene detected using real-time PCR. The figure shows a melting temperature of β-actin gene as 84.86°C with no amplifications detected in negative controls.

5. Discussion

The self-renewal and differentiation of spermatogonia stem cells (SSCs) into sperm is known as spermatogenesis. Male infertility can result from any error that occurs during spermatogenesis. Male factors account for 50% of cases of infertility, which affects 10-15 percent of all couples(1,19). One factor that contributes to male infertility is high temperature. Temporary heat stress can alter sperm motility, life cycle, energy metabolism, sperm count, and sperm volume(19,20). According to our result, scrotal hyperthermia which was induced on mice showed a significant decrease on sperm count, mortality and its viability. Several evidence indicates that apoptosis is involved in both spontaneous (during normal spermatogenesis) and increased germ cell death which is triggered by a variety of regulatory stimuli. Rat models have been utilized in prior studies to investigate the impact of several cell death mechanisms in heat-induced germ cell death in the testis (8,20–22). The current study aimed to examine indicators of the newly discovered non-apoptotic, caspase-independent cell death pathways related to sperm loss after hyperthermia. Using azoospermia animal models, our results characterize the molecular pathways involved in heat-induced cell death in testicular tissue. To test this hypothesis, ten selected mice were exposed to a temperature of 43°C for 20 minutes every other day for 5 weeks. All of them exhibited decreases in sperm parameters such as sperm count, motility, viability, and normal morphology compared to the control group. Testicular weight, testicular volume, and seminiferous tubule length were significantly lower in the hyperthermia group than in the control group. Based on the results of the stereological examination, all seminiferous tubules were severely degenerated and devoid of spermatogenic cells, and all mice in the hyperthermia group had azoospermia. To investigate the reasons behind germ cell degeneration and the reduction in the number of spermatogenic cells in heat-induced mice, the current study assessed the role of two newly identified routes of regulated cell death, namely alkaliptosis and oxeiptosis, in hyperthermia-mediated testicular injury in an animal model.

Alkaliptosis is a type of regulated cell death induced by intracellular alkalinization. Historically, this pathway was recognized during attempts to screen for the cytotoxic activity of small-molecule compounds targeting G-protein coupled receptors(10). The cytotoxic effects of the identified agent, JTC801, did not depend on any known cell death pathways, including apoptosis, necroptosis, autophagy, or ferroptosis. However, these effects were blocked by the suppression of intracellular alkalinization using N-acetyl cysteine, N-acetyl alanine, and acidic culture media(10).Molecular studies have revealed the involvement of the ikbkb gene in this pathway.

Notably, the ikbkb-nf-κB-mediated downregulation of ca9 was found to be a key event in this cytotoxic pathway (10,23,24). The observed downregulation of ca9 and unchanged levels of Ikbkb in the hyperthermia group suggest the involvement of alkaliptosis in the hyperthermia-induced changes in the testes.

Oxeiptosis is another route of regulated cell death that depends on oxygen radicals and is stimulated by the induction of the keap1-pgam5-aifm1 axis(9). This novel pathway was identified in an animal study demonstrating the response of mice to ozone. Ozone-induced oxeiptosis was found to be independent of apoptotic or pyroptotic caspases, necroptosis, autophagic pathways, and ferroptosis(9,23). The results of the current study showed a significant upregulation of the keap1 and pgam5 genes, along with a remarkable downregulation of aifm1 levels in the animals exposed to hyperthermia. Thus, oxeiptosis might also be involved in the hyperthermia-induced changes in the mice. In line with our study, a recent investigation demonstrated upregulation of KEAP1 and PGAM5 proteins in the TM4 cells (testicular sertoli cell line) treated with the TDCIPP toxic substance. While this toxic agent also led to upregulation of AIFM1 protein, the relative expression of p-AIFM1 protein was lower in the treated animals compared with the controls. Taken together, the authors concluded that the TDCIPP-induced decrease in the viability of TM4 cells might be related to ROS-mediated regulation of the keap1-pgam5-aifm1 pathway, resulting in oxeiptosis(24).

According to a study, the expression of 61 proteins can be dysregulated as a result of heat stress. These proteins serve various functions in the cell pathway(25). Many of these regulations derive their pathogenesis in large part from oxidative stress. Oxidative stress is an imbalance between the body's antioxidant defense systems and the production of reactive oxygen species (ROS). There are many different molecules in the ROS family that have varying effects on cellular function(25,26). ROS is not the only source of protein damage and alteration; acid-base homeostasis can also lead to cell death in various situations(27). Acid denaturation of sperm chromatin structure has been observed in response to a single, mild, transient heat stress of the scrotum(28–30). Loss of the Na/H (NHE) exchangers responsible for pH modification in the testes has been shown to cause male infertility. Overexpression or knockdown of NHEs causes alkalinization or acidification of the organelle lumen. pH modifiers are required in germ cells for intact acrosomiogenesis, sperm development, and male fertility(31). Research into agents that cause cell death in a pH-dependent manner has discovered a new pathway known as alkaliptosis(10). Induction of alkaliptosis begins with an opioid analgesic called JTC801. This compound induces alkaliptosis in cancer cells by activating nf-κb (nuclear factor kappa B), which

represses the expression of the carbonic anhydrase 9 gene (ca9) responsible for pH balance in cells(32). Redox imbalance, decreased sperm motility, and DNA damage are the consequences of elevated ROS and diminished antioxidant defense. Due to the high concentration of unsaturated fatty acids in their cell membranes, spermatozoa are particularly vulnerable to ROS's damaging effects. The intracellular oxidative burden is exacerbated by reactive oxygen species, which aid in the peroxidation of lipids. Several intrinsic and extrinsic factors have been linked to increase oxidative stress in the male reproductive system. The sequence of events includes lipid peroxidation, loss of membrane integrity with increased permeability, decreased sperm motility, structural DNA damage, and apoptosis(33). The human spermatozoa are highly susceptible to oxidative stress, high levels of free radicals, and ROS, including the superoxide anion and hydrogen peroxide(34,35). Oxidative stress can be deleterious and cause oxidative damage to the sperm plasma membrane and DNA fragmentation of both the nuclear and mitochondrial genomes. Although oxidative stress has been investigated in animal models and cryptorchidism and varicocele patients, it was originally proposed that apoptosis causes cell death in response to transient heat(10,36). The proportion of sperm with destroyed mitochondrial membranes increased after hyperthermia, and higher levels of activated caspase proteins and an alteration in the Fas/FasL signaling pathway were detected(37,38). Oxidative stress has always been considered as the source of triggering the apoptotic pathway. It has been shown that oxidative stress can be a key factor in impaired spermatogenesis due to cryptorchidism, varicocele, or mild hyperthermia(39).

During the ontogeny of the testis, apoptosis can occur at any time, but it is most common during spermatogenesis. Apoptosis and cell survival are influenced by a wide range of factors, including growth factors (such as stem cell factor [SCF], fibroblast growth factor [FGF], and tumor growth factor [TGF]), hormones (including follicle-stimulating hormone [FSH], luteinizing hormone [LH], estradiol [E2], and Müllerian-inhibiting substance [MIS]), partial oxygen pressure, and testis-specific genes. The types of stimuli received by the germinal centers and sperm determine the apoptosis pathways they utilize. In heat-stress-induced apoptosis, various intrinsic and extrinsic pathways are initiated(40). Previous research on the Bcl-2 (B-cell lymphoma 2) protein family has shed light on the mechanisms of apoptosis. It is generally accepted that the most important factor in determining a cell's fate is the ratio of Bcl-2 family proteins that promote and inhibit apoptosis. An excess of Bcl-2 results in cell survival, while an excess of Bax leads to cell death(41). Extrinsic apoptosis in spermatogenic cells, particularly elongating and mature sperm, is mediated by the FasL (Fas ligand)-Fas system and the TRAIL (TNF-related apoptosis-inducing ligand)-DR4/DR5 system. The type I transmembrane receptor Fas (Apo/CD95), expressed in germinal centers, is

a member of the TNF/NGFR (nerve growth factor receptor) superfamily and initiates apoptosis by binding to FasL, which is expressed in Sertoli cells. In Sertoli cells, TRAIL, a type II transmembrane protein, binds to its receptors, DR4 (TRAIL-R1/TNFRSF10A) and/or DR5 (TRAIL-R2/TNFRSF10B), in a manner that is analogous to the FasL-Fas system. The Cdc42/apoptosis signal-regulating kinase 1/c-Jun N-terminal kinase pathway may be responsible for triggering FasL expression in resveratrol-induced HL-60 cells, and similar events may occur in germ cells. The adaptor molecule FADD (Fas-associated death domain) quickly identifies and binds to the death domains of the receptors, resulting in the formation of a trimeric receptor. The complex known as DISC (Death-Inducing Signaling Complex) is formed when activated FADD recruits the precursor Caspase 8. DISC is eliminated by processed Caspase 8, leading to the activation of effector Caspases 3, 6, or 7, which degrade a large number of cellular proteins and cause cell death(5,37,40–42). According to Lin and Richburg mice lacking the trail gene (trail-/-) have a significantly lower testis-to-body weight ratio, an elevated apoptotic index, increased levels of cleaved Caspase 8 and 9, and a reduced sperm head count. All of these results indicate that Trail is necessary for normal spermatogenesis and that the FasL-Fas system and intrinsic pathway compensate for disturbances in homeostasis(42). Non-apoptotic pathways of cell death are also activated by oxidative stress. For example, oxidative stress can stimulate pyroptosis and necroptosis, while parthanatos begins with oxidative DNA damage, and ferroptosis can be triggered by iron-dependent ROS production(5)s. In a previous study on the effect of scrotal hyperthermia on infertility, it was found that the protein expression of cell death markers such as Caspase-1, Beclin-1, Atg7, MLKL, and Acsl4 increased, serving as non-apoptotic cell death biomarkers for necroptosis, pyroptosis, ferroptosis, and autophagy(8). However, it appears that sperm loss after hyperthermia is even more complicated and crosstalk of these non-apoptotic pathways cannot fully explain the whole process.

Sertoli cells control and support spermatogenesis, which is essential for male fertility. Their functions include the formation of the blood–testis barrier, the production of seminiferous tubular fluid and the secretion of factors necessary for the development of the germ cell line. Sertoli cells are primarily responsible for the distinct composition of seminiferous tubular fluid in the male reproductive tract compared to blood and other body fluids(43). These cells regulate the pH and ionic composition of seminiferous tubular fluid through several enzymes and transporters. HCO_3^- serves as the primary mobile physiological buffer, protecting cells from fluctuations in luminal fluids and intracellular pH. This ion is crucial for male reproduction, as evidenced by the presence of HCO_3^- transporters in the male reproductive tract. Changes in HCO_3^- concentration and pH in Sertoli cells can affect the ionic balance of the male reproductive tract, potentially leading to

subfertility or infertility(43–45). Studies have shown that certain enzymes specifically CAs may influence the unique microenvironment of cells by maintaining an acidic extracellular pH, which facilitates cell growth(46). CAs vary in their subcellular and tissue localization and are widely dispersed in living organisms. The kinetic properties, inhibitor sensitivity, and selectivity of CAs' isozymes also vary. In humans, fifteen distinct isoforms have been identified, primarily distinguished by their subcellular localization. Isoforms IX, XII, and XIV are transmembrane, while CA I, CA II, CA III, CA VII, CA VIII, CA X, CA XI, and CA XIII are cytosolic. CA IV and CA VI are bound to the cell membrane. The only mitochondrial isoforms are CA V (A and B) and CA VI(47). While variant CA VA is found exclusively in hepatocytes, variant CA VB is present in a broader range of tissues. Several metabolic pathways, such as gluconeogenesis, lipogenesis, and ureagenesis, are believed to be regulated by CA V. It is important to consider that even when CAs are inhibited, HCO_3^- formation is not completely suppressed; however, its production is significantly reduced because CAs facilitate CO_2 hydration(48–50). The presence of HCO_3^- transporters in Sertoli cell membranes may also contribute to maintaining an appropriate ionic balance between the intracellular and extracellular environments(51). The inhibition of all CAs in Sertoli cells could lead to a decrease in the expression of genes related to mitochondrial biogenesis(52). Inhibition of CA The increased abundance of hormone-sensitive lipase (HSL) in Sertoli cells indicates that CA inhibition also alters lipid metabolism(52). Interestingly, HSL is found in only Sertoli cells and germ cells rather than in Leydig cells in rats and mice, which are responsible for steroid production. Male HSL knockout mice are sterile, exhibit oligospermia, and have elevated cholesterol esters in their testes(53,54). The testis's first line of defense against bacteria and viruses is a family of pattern recognition receptors called toll-like receptors (TLRs). TLRs were initially thought to recognize only specific bacteria, but it has since been shown that they can be activated by many signals induced by stress or cell injury(55). MyD88, an adaptor protein, mediates common TLR signaling by recruiting other intermediate molecules that, in turn, activate IκB. This degradation releases NF-κB for translocation into the nucleus, where it induces the transcription of cytokines such as interleukin (IL)-1, IL-2, IL-4, and tumor necrosis factor (TNF-α) in response to TLR activation(55,56). Although some studies have demonstrated that inhibition of the NF-κB signaling pathway prevents THS26-induced testicular injury, the mechanism behind this effect has not been fully explained(57). Maintaining spermatogenesis is one of the important functions of the testosterone. Through the androgen receptor (AR) pathway, testosterone activates Akt signaling and regulates cell proliferation and apoptosis(58). In addition, there is evidence that testosterone downregulates the expression of TNF-α in endothelial cells and inhibits the NF-κB signaling pathway(59). Testosterone has also been shown to downregulate TLR4 in

prostate smooth muscle cells, inhibiting NF-κB activation and lowering IL-1 and TNF-α expression(60). A heat-resistant glycoprotein known as erythropoietin (EPO) has been shown to activate Akt, which in turn acts as an anti-apoptotic agent. Additionally, it has been reported that EPO inhibits the TLR4/NF-κB signaling pathway, thereby acting as an anti-inflammatory agent in crush syndrome-induced acute renal inflammation and lung ischemia/reperfusion-induced inflammation(57,61). It has been demonstrated that the Tyro-3, Axl, and Mer (TAM) family of tyrosine kinase receptors negatively regulate the TLR/NF-κB signaling pathway, making them important testicular immune regulatory factors. However, it is still unknown whether testosterone, EPO, or TAM receptors are involved in the dysregulation of spermatogenesis caused by THS(62). According to previous research, the THS-induced spermatogenesis deficit is accompanied by a brief drop in serum testosterone and increases in FSH and LH levels. The inhibition of steroidogenesis by THS was attributed to the decrease in testosterone and its receptor, AR, which exhibited significantly lower expression levels following THS exposure(63). Spermatogenesis takes place in the seminiferous tubules. In Sertoli cells, testosterone regulates spermatogenesis solely by binding to AR. Since AR-expressing Leydig cells are less sensitive to testosterone levels than other cells, the expression of AR did not significantly decrease as testosterone levels declined. However, testosterone levels recover two weeks after acute THS exposure through a compensatory production mechanism, so the small effect of THS on testosterone content can be overlooked(57,63). Our analysis showed that the relative expression of NF-κB was significantly higher, and the expression of the CA9 gene was significantly lower in the scrotal hyperthermia group. The relative expression of the IKBKB gene did not change significantly between the scrotal hyperthermia and control groups.

The AIF gene, also known as AIFM1 and PCDC8, is mapped to the Xq25–26 region on human chromosome 4 and in mice. A 67 kDa precursor molecule containing the N-terminal mitochondrial leading sequence (MLS), two nuclear leading sequences (NLS), and NAD- and FAD-binding motifs is produced by the nuclear-encoded gene during transcription and translation(64). The precursor can only be transported to mitochondria in a non-native form, preventing or delaying its folding in the cytoplasm. Full-length AIF becomes apoptogenic upon refolding, regardless of whether FAD is bound. Apoptosis-inducing factor 1 (AIF1) functions both as an NADH oxidoreductase and as a regulator of apoptosis. In response to apoptotic stimuli, it is released from the mitochondrial intermembrane space into the cytosol and the nucleus, where it acts as a pro-apoptotic factor in a caspase-independent pathway. Conversely, it functions as an anti-apoptotic factor in normal mitochondria via its NADH oxidoreductase activity. The soluble form (AIFsol) found in the nucleus induces "parthanatos," a caspase-independent fragmentation of

chromosomal DNA. This gene encodes a flavoprotein essential for nuclear disassembly in apoptotic cells, and it is located in the mitochondrial intermembrane space in healthy cells. Induction of apoptosis results in the translocation of this protein to the nucleus, where it influences chromosome condensation and fragmentation. Additionally, this gene product prompts mitochondria to release the apoptogenic proteins cytochrome c and caspase-9(64). Our analysis showed that the relative expression of the AIFM1 gene was significantly lower in the scrotal hyperthermia group.

A master regulator of cellular oxidative and electrophilic stress responses, nuclear factor erythroid 2 like 2 (nfe2l2), also known as nrf2, is a transcription factor. Several antioxidant defense mechanisms are regulated by nfe2l2, which impacts ROS homeostasis. The DNA sequence known as the antioxidant response element (ARE) is involved in the homeostatic control of oxidants in the nfe2l2 target genes. Nfe2l2 is prevented from activating its target genes when kelch-like ECH-associated protein 1 (keap1) binds to it and sequesters it from the nucleus during the basal state(65,66). On the other hand, nfe2l2 escapes proteasomal degradation, stabilizes, translocates to the nucleus, and activates its target genes when stressed. The conserved oxidative stress defense mechanism is the keap1-nfe2l2 system. Nfe2l2 regulates inflammation and protects against oxidative stress(65–67). In nrf2 knockout mice, it was reported that inflammatory biomarkers like interleukin (IL) 1b, IL6, tumor necrosis factor alpha (tnfa), and prostaglandin-endoperoxide synthase 2 (ptgs2) were induced. The expression of nfe2l2 and these cytokine genes is closely linked(68). A previous study on the induction of oxidative stress and activation of the keap1-nfe2l2-ARE pathway in bovine endometrial epithelial cells demonstrated that under heat stress, the keap1–nfe2l2 pathway induces antioxidant enzymes, contributing to oxidative stress resistance. After 15 hours of heat stress, the mRNA expression levels of antioxidant enzymes, potential targets of nfe2l2, gradually increased and were significantly high(69). According to these findings, heat-stressed bovine endometrial epithelial cells upregulated the ARE-dependent antioxidant enzyme genes by stabilizing nfe2l2. Moreover, in bovine endometrial epithelial cells cultured at both low and high temperatures, keap1 and nfe2l2 proteins were detected by immunostaining. Under normal conditions, nfe2l2 was primarily found in the nucleus, whereas under heat-stress conditions, it was found in both the cytoplasm and the nucleus. Bovine endometrial epithelial cells cultured under heat stress appear to benefit from the protective role played by the keap1-nfe2l2-ARE pathway, as indicated by these findings. Modifying the keap1-nfe2l2-ARE pathway in bovine endometrial epithelial cells may help mitigate the adverse effects of heat and oxidative stress(69). In 2020, a study examined the connection between nrf2 and apoptosis in mice before adulthood. Their findings demonstrated that nrf2

suppresses oxidative stress in the testes of mice at various developmental stages prior to adulthood. Puberty is an important time for the development of the mammalian reproductive system. The male reproductive system is more susceptible to external factors during puberty, which can alter reproductive function. After eight weeks of age, mice become adults. The researchers discovered that the spermatogenic tubule diameter in mouse testes sharply increased before adulthood, and that absolute and relative testis weights increased with age in mice. In addition, histological examinations revealed that the various types of spermatogenic cells in the seminiferous tubules increased with age, with spermatogonia predominating at one week of age(70). The expression of pgp9.5 also increased with age. Taken together, these findings demonstrated that spermatogenic cells in the mouse testis experienced rapid proliferation prior to adulthood. Several studies have shown that mitochondrion-derived reactive oxygen species (ROS) and lipid peroxidation of the cell membrane can cause spermatogenic cells to undergo apoptosis and die(71). MDA (malondialdehyde) and antioxidant production rise in response to increased oxidative stress. MDA levels increase due to decreased antioxidant enzyme activity in mouse testis tissue, leading to damage in the testis. Additionally, the arrangement of spermatogenic cells is disrupted and the structures of cells in testicular tissue, such as mitochondria, are damaged as MDA levels rise. During spermatogenesis, oxidative stress is largely mitigated by nrf2, a basic leucine zipper transcription factor. Keap1 is responsible for nrf2, and the nrf2/keap1 antioxidant response element pathway is a crucial antioxidant defense system. Nrf2 expression rises in response to oxidative stress, allowing nrf2 to move from the cytoplasm to the nucleus. The two antioxidant enzymes NQO-1 and HO-1 are activated downstream of the oxidative stressor as a result of this protein's interaction with the antioxidant response element(72). In this study, the keap1 gene showed a significant increase in the scrotal hyperthermia group compared to the control group without heat stress.

To maintain cell physiology and homeostasis, the mitochondria of germ cells require substantial energy and dynamic mitochondrial activity. Mitochondria are highly dynamic organelles that constantly move, fuse, and divide in response to changes in the energy demands of the cell. The large dynamin GTPases embedded in the mitochondrial membrane (DRP1, OPA1, MFN1, and MFN2) regulate mitochondrial dynamics(73). According to Twig et al., mitochondrial fission promotes the degradation and elimination of damaged mitochondria while also generating new mitochondria, which are essential for cell growth. To meet dynamic energy demands, mitochondrial fusion ensures that organelles complement one another closely(73). According to Yu et al., the mitochondrial protein phosphatase phosphoglycerate mutant enzyme family member 5 (PGAM5) is involved in various stress responses, including cell death and mitochondrial quality

control(74). The mitochondria, which are the largest energy storage organelles in cells, contain the OXPHOS protein that synthesizes ATP and the β-oxidase used for fuel transport. The mitochondria face metabolic challenges when the human body is subjected to stress that disrupts energy homeostasis. By promoting DRP1's mitochondrial translocation and dephosphorylating DRP1 at S637, PGAM5 initiates mitochondrial fission(75). Numerous studies have confirmed PGAM5's involvement in the development of Parkinson's disease, acute kidney injury, and hepatitis. However, PGAM5's role in the regulation of aging germ cells remains unclear. Current studies suggest that oocytes and mitochondrial dynamics play significant roles. Notably, PGAM5 is also involved in the lysis of mitochondria, which is a novel finding from previous research(76). The formation of the BAX/PGAM5/DRP1 complex is necessary for the execution of endogenous mitochondrial apoptosis, and previous studies have confirmed that PGAM5 can promote the translocation of BAX to mitochondria and the dephosphorylation of DRP1(77). PGAM5, DRP1, and BAX are multimers found in the cytoplasm. They are drawn to the mitochondria by receptors on the outer mitochondrial membrane, where they facilitate mitochondrial division in cells. In aging germ cells, excessive mitochondrial division leads to abnormal metabolic function and a decline in energy. A recent study examining the correlation of PGAM5 with aging in oocytes demonstrated a negative correlation between PGAM5 and DRP1 regarding the rate of fertilization and the number of fertilized eggs in CC patients experiencing infertility(76). In the current study, the relative expression level of pgam5 was assessed by qRT-PCR, showing a significant upregulation of this gene in the scrotal hyperthermia group compared to the control group without stress.

6. Conclusion

In summary, the process of cell death in response to scrotal hyperthermia is complex. Our results support the role of a newly discovered non-apoptotic cell death pathway, alkaliptosis and oxeiptosis, in sperm count and testicular volume reduction in response to heat stress. Furthermore, our findings demonstrated that apoptosis was induced by heat stress in mouse testes by a significant up-regulation of keap1, nf-κb and pgam5 genes, while ca9, and aifm1 showed a remarkable down-regulation in the studies groups. Our findings establish that these genes might have protective role in male fertility and shed light on the age-related oxidative stress-mediated impairment of spermatogenesis in mouse testes.

7. References

1. Franken DR, Oehninger S. Semen analysis and sperm function testing. Asian J Androl. 2012 Jan;14(1):6–13.

2. Liu XZ, Tang YG, Liu H, Tang LX, Wen RQ. [Relationship between testis volume and types of spermatogenic cells from testicular biopsy in patients with azoospermia or cryptozoospermia]. Zhonghua Nan Ke Xue. 2010 Jan;16(1):52–4.

3. Morgentaler A, Stahl BC, Yin Y. Testis and temperature: an historical, clinical, and research perspective. J Androl. 1999 Apr;20(2):189–95.

4. Park W, Wei S, Kim BS, Kim B, Bae SJ, Chae YC, et al. Diversity and complexity of cell death: a historical review. Exp Mol Med. 2023 Aug 1;55(8):1573–94.

5. Tang D, Kang R, Berghe TV, Vandenabeele P, Kroemer G. The molecular machinery of regulated cell death. Cell Res. 2019 May 1;29(5):347–64.

6. Pirani M, Novin MG, Abdollahifar MA, Piryaei A, Kuroshli Z, Mofarahe ZS. Protective Effects of Fisetin in the Mice Induced by Long-Term Scrotal Hyperthermia. Reprod Sci. 2021 Nov 1;28(11):3123–36.

7. Khosravi A, Hasani A, Behnam P, Piryaei A, Pirani M, Aliaghaei A, et al. An effective method for establishing animal models of azoospermia and oligospermia. Andrologia. 2021 Aug;53(7): e14095.

8. Hasani A, Khosravi A, Behnam P, Ramezani F, Eslami Farsani B, Aliaghaei A, et al. non-apoptotic cell death such as pyroptosis, autophagy, necroptosis and ferroptosis acts as partners to induce testicular cell death after scrotal hyperthermia in mice. Andrologia. 2022 Mar;54(2):e14320.

9. Holze C, Michaudel C, Mackowiak C, Haas DA, Benda C, Hubel P, et al. Oxeiptosis, a ROS-induced caspase-independent apoptosis-like cell-death pathway. Nat Immunol. 2018 Feb;19(2):130–40.

10. Liu J, Kuang F, Kang R, Tang D. Alkaliptosis: a new weapon for cancer therapy. Cancer Gene Ther. 2020 May;27(5):267–9.

11. Ziaeipour S, Rezaei F, Piryaei A, Abdi S, Moradi A, Ghasemi A, et al. Hyperthermia versus busulfan: Finding the effective method in animal model of azoospermia induction. Andrologia. 2019 Dec;51(11):e13438.

12. Afshar A, Aliaghaei A, Nazarian H, Abbaszadeh HA, Naserzadeh P, Fathabadi FF, et al. Curcumin-Loaded Iron Particle Improvement of Spermatogenesis in Azoospermic Mouse Induced by Long-Term Scrotal Hyperthermia. Reprod Sci. 2021 Feb;28(2):371–80.

13. Heidari F, Kian N, Azad N, Chiti H, Freidouni M, Fakheri F, et al. Age-related histopathological and biochemical testicular damages were ameliorated by vitamin C administration. Rev Int Androl. 2023 Jun;21(2):100327.

14. Shadmehr S, Fatemi Tabatabaei SR, Hosseinifar S, Tabandeh MR, Amiri A. Attenuation of heat stress-induced spermatogenesis complications by betaine in mice. Theriogenology. 2018 Jan 15; 106:117–26.

15. Ghaffari Novin M, Sabbagh Alvani M, Mafi Balani M, Aliaghaei A, Afshar A, Aghajanpour F, et al. Therapeutic Effects of Edaravone on Azoospermia: Free Radical Scavenging and Autophagy Modulation in Testicular Tissue of Mice. J Reprod Infertil. 2022;23(2):73–83.

16. Dehghani F, Hassanpour A, Poost-Pasand A, Noorafshan A, Karbalay-Doust S. Protective effects of L-carnitine and homogenized testis tissue on the testis and sperm parameters of busulfan-induced infertile male rats. Iran J Reprod Med. 2013 Sep;11(9):693–704.

17. Majd E, Nejad G. Stereological study of Arabian ram testis during different seasons. Iran J Vet Res. 2009;10(4).

18. Brown DL. Bias in image analysis and its solution: unbiased stereology. J Toxicol Pathol. 2017;30(3):183–91.

19. Al-Otaibi ST. Male infertility among bakers associated with exposure to high environmental temperature at the workplace. J Taibah Univ Med Sci. 2018 Apr;13(2):103–7.

20. Kanter M, Aktas C, Erboga M. Heat stress decreases testicular germ cell proliferation and increases apoptosis in short term: an immunohistochemical and ultrastructural study. Toxicol Ind Health. 2013 Mar;29(2):99–113.

21. Hikim APS, Lue Y, Yamamoto CM, Vera Y, Rodriguez S, Yen PH, et al. Key Apoptotic Pathways for Heat-Induced Programmed Germ Cell Death in the Testis. Endocrinology. 2003 Jul;144(7):3167–75.

22. Vera Y, Diaz-Romero M, Rodriguez S, Lue Y, Wang C, Swerdloff RS, et al. Mitochondria-Dependent Pathway Is Involved in Heat-Induced Male Germ Cell Death: Lessons from Mutant Mice1. Biol Reprod. 2004 May 1;70(5):1534–40.

23. Scaturro P, Pichlmair A. Oxeiptosis-a cell death pathway to mitigate damage caused by radicals. Cell Death Differ. 2018 Jul;25(7):1191–3.

24. Wang L, Quan C, Liu S, Sun Y, Liu Y, Zhang L. [KEAP1/PGAM5/AIFM1 mediated oxeiptosis pathway in TDCIPP-induced reduction of TM4 cell viability]. Wei Sheng Yan Jiu. 2023 Nov;52(6):979–92.

25. Wu YQ, Rao M, Hu SF, Ke DD, Zhu CH, Xia W. Effect of transient scrotal hyperthermia on human sperm: an iTRAQ-based proteomic analysis. Reprod Biol Endocrinol. 2020 Dec;18(1):83.

26. Barati E, Nikzad H, Karimian M. Oxidative stress and male infertility: current knowledge of pathophysiology and role of antioxidant therapy in disease management. Cell Mol Life Sci. 2020 Jan;77(1):93–113.

27. Moloney JN, Cotter TG. ROS signalling in the biology of cancer. Semin Cell Dev Biol. 2018 Aug; 80:50–64.

28. Martínez-Pastor F, Del Rocío Fernández-Santos M, Domínguez-Rebolledo Á, Esteso M, Garde J, Biology of Reproduction Group. DNA Status on Thawed Semen from Fighting Bull: A Comparison Between the SCD and the SCSA Tests. Reprod Domest Anim. 2009 Jun;44(3):424–31.

29. Loi P, Fulka J, Hildebrand T, Ptak G. Genome of non-living cells: trash or recycle? REPRODUCTION. 2011 Oct;142(4):497–503.

30. Balasuriya A, Serhal P, Doshi A, Harper JC. Processes involved in assisted reproduction technologies significantly increase sperm DNA fragmentation and phosphatidylserine translocation. Andrologia. 2014 Mar;46(2):86–97.

31. Ahmad G, Moinard N, Esquerré-Lamare C, Mieusset R, Bujan L. Mild induced testicular and epididymal hyperthermia alters sperm chromatin integrity in men. Fertil Steril. 2012 Mar;97(3):546–53.

32. Song X, Zhu S, Xie Y, Liu J, Sun L, Zeng D, et al. JTC801 Induces pH-dependent Death Specifically in Cancer Cells and Slows Growth of Tumors in Mice. Gastroenterology. 2018 Apr;154(5):1480–93.

33. Henkel R, Schill WB. Sperm separation in patients with urogenital infections. Andrologia. 2009 Apr 27;30(S1):91–7.

34. Panner Selvam MK, Agarwal A, Henkel R, Finelli R, Robert KA, Iovine C, et al. The effect of oxidative and reductive stress on semen parameters and functions of physiologically normal human spermatozoa. Free Radic Biol Med. 2020 May; 152:375–85.

35. Aitken RJ, Drevet JR. The Importance of Oxidative Stress in Determining the Functionality of Mammalian Spermatozoa: A Two-Edged Sword. Antioxidants. 2020 Jan 27;9(2):111.

36. Zhang MH, Zhang AD, Shi ZD, Wang LG, Qiu Y. Changes in Levels of Seminal Nitric Oxide Synthase, Macrophage Migration Inhibitory Factor, Sperm DNA Integrity and Caspase-3 in Fertile Men after Scrotal Heat Stress. Schlatt S, editor. PLOS ONE. 2015 Oct 29;10(10): e0141320.

37. Xu YR, Dong HS, Yang WX. Regulators in the apoptotic pathway during spermatogenesis: Killers or guards? Gene. 2016 May;582(2):97–111.

38. Rao M, Xia W, Yang J, Hu L -X., Hu S -F., Lei H, et al. Transient scrotal hyperthermia affects human sperm DNA integrity, sperm apoptosis, and sperm protein expression. Andrology. 2016 Nov;4(6):1054–63.

39. Rao M, Zhao XL, Yang J, Hu SF, Lei H, Xia W, et al. Effect of transient scrotal hyperthermia on sperm parameters, seminal plasma biochemical markers, and oxidative stress in men. Asian J Androl. 2015;17(4):668.

40. Teijido O, Dejean L. Upregulation of Bcl2 inhibits apoptosis-driven BAX insertion but favors BAX relocalization in mitochondria. FEBS Lett. 2010 Aug 4;584(15):3305–10.

41. Lizama C, Alfaro I, Reyes JG, Moreno RD. Up-regulation of CD95 (Apo-1/Fas) is associated with spermatocyte apoptosis during the first round of spermatogenesis in the rat. Apoptosis. 2007 Feb 15;12(3):499–512.

42. Lin YC, Richburg JH. Characterization of the Role of Tumor Necrosis Factor Apoptosis Inducing Ligand (TRAIL) in Spermatogenesis through the Evaluation of Trail Gene-Deficient Mice. Bratton SB, editor. PLoS ONE. 2014 Apr 15;9(4): e93926.

43. Richburg JH, Redenbach DM, Boekelheide K. Seminiferous Tubule Fluid Secretion Is a Sertoli Cell Microtubule-Dependent Process Inhibited by 2,5-Hexanedione Exposure. Toxicol Appl Pharmacol. 1994 Oct;128(2):302–9.

44. Swietach P, Hulikova A, Vaughan-Jones RD, Harris AL. New insights into the physiological role of carbonic anhydrase IX in tumour pH regulation. Oncogene. 2010 Dec 16;29(50):6509–21.

45. Supuran CT. Carbonic anhydrase inhibitors and their potential in a range of therapeutic areas. Expert Opin Ther Pat. 2018 Oct 3;28(10):709–12.

46. Ivanov S, Liao SY, Ivanova A, Danilkovitch-Miagkova A, Tarasova N, Weirich G, et al. Expression of Hypoxia-Inducible Cell-Surface Transmembrane Carbonic Anhydrases in Human Cancer. Am J Pathol. 2001 Mar;158(3):905–19.

47. Supuran CT. Carbonic anhydrase inhibitors and their potential in a range of therapeutic areas. Expert Opin Ther Pat. 2018 Oct 3;28(10):709–12.

48. Geers C, Gros G. Carbon Dioxide Transport and Carbonic Anhydrase in Blood and Muscle. Physiol Rev. 2000 Jan 4;80(2):681–715.

49. Nishimori I, Vullo D, Innocenti A, Scozzafava A, Mastrolorenzo A, Supuran CT. Carbonic Anhydrase Inhibitors. The Mitochondrial Isozyme VB as a New Target for Sulfonamide and Sulfamate Inhibitors. J Med Chem. 2005 Dec 1;48(24):7860–6.

50. Scozzafava A, Supuran CT, Carta F. Antiobesity carbonic anhydrase inhibitors: a literature and patent review. Expert Opin Ther Pat. 2013 Jun;23(6):725–35.

51. Bernardino RL, Costa AR, Martins AD, Silva J, Barros A, Sousa M, et al. Estradiol modulates Na^+ -dependent HCO_3^- transporters altering intracellular pH and ion transport in human Sertoli cells: A role on male fertility? Biol Cell. 2016 Jul;108(7):179–88.

52. Bernardino RL, Dias TR, Moreira BP, Cunha M, Barros A, Oliveira E, et al. Carbonic anhydrases are involved in mitochondrial biogenesis and control the production of lactate by human Sertoli cells. FEBS J. 2019 Apr;286(7):1393–406.

53. Casado ME, Huerta L, Ortiz AI, Pérez-Crespo M, Gutiérrez-Adán A, Kraemer FB, et al. HSL-knockout mouse testis exhibits class B scavenger receptor upregulation and disrupted lipid raft microdomains. J Lipid Res. 2012 Dec;53(12):2586–97.

54. Kraemer FB, Shen WJ. Hormone-sensitive lipase. J Lipid Res. 2002 Oct;43(10):1585–94.

55. Gárate I, Garcia-Bueno B, Madrigal JLM, Caso JR, Alou L, Gomez-Lus ML, et al. Stress-Induced Neuroinflammation: Role of the Toll-Like Receptor-4 Pathway. Biol Psychiatry. 2013 Jan;73(1):32–43.

56. Chen X, Zhang C, Wang X, Huo S. Juglanin inhibits IL-1β-induced inflammation in human chondrocytes. Artif Cells Nanomedicine Biotechnol. 2019 Dec 4;47(1):3614–20.

57. Hu SQ, Liu DL, Li CR, Xu YH, Hu K, Cui LD, et al. Wuzi-Yanzong prescription alleviates spermatogenesis disorder induced by heat stress dependent on Akt, NF-κB signaling pathway. Sci Rep. 2021 Sep 22;11(1):18824.

58. Li D, Wang Q, Shi K, Lu Y, Yu D, Shi X, et al. Testosterone Promotes the Proliferation of Chicken Embryonic Myoblasts Via Androgen Receptor Mediated PI3K/Akt Signaling Pathway. Int J Mol Sci. 2020 Feb 9;21(3):1152.

59. Jin H, Qiu WB, Mei YF, Wang DM, Li YG, Tan XR. Testosterone alleviates tumor necrosis factor-alpha-mediated tissue factor pathway inhibitor downregulation via suppression of nuclear factor-kappa B in endothelial cells. Asian J Androl. 2009 Mar;11(2):266–71.

60. Leimgruber C, Quintar AA, García LN, Petiti JP, De Paul AL, Maldonado CA. Testosterone abrogates TLR4 activation in prostate smooth muscle cells contributing to the preservation of a differentiated phenotype. J Cell Physiol. 2013 Jul;228(7):1551–60.

61. He Q, Zhao X, Bi S, Cao Y. Pretreatment with Erythropoietin Attenuates Lung Ischemia/Reperfusion Injury via Toll-Like Receptor-4/Nuclear Factor-κB (TLR4/NF-κB) Pathway. Med Sci Monit. 2018 Mar 1; 24:1251–7.

62. Gilchrist SE, Goudarzi S, Hafizi S. Gas6 Inhibits Toll-Like Receptor-Mediated Inflammatory Pathways in Mouse Microglia via Axl and Mer. Front Cell Neurosci. 2020; 14:576650.

63. Lue YH, Lasley BL, Laughlin LS, Swerdloff RS, Hikim APS, Leung A, et al. Mild testicular hyperthermia induces profound transitional spermatogenic suppression through increased germ cell apoptosis in adult cynomolgus monkeys (Macaca fascicularis). J Androl. 2002;23(6):799–805.

64. Sevrioukova IF. Apoptosis-Inducing Factor: Structure, Function, and Redox Regulation. Antioxid Redox Signal. 2011 Jun 15;14(12):2545–79.

65. Yi T, Li X, Wang E, Zhang Y, Fu Y, Li J, et al. Activation of the Nuclear Erythroid 2-Related Factor 2 Antioxidant Responsive Element (Nrf2-ARE) Signaling Pathway Alleviates Acute Graft-Versus-Host Disease by Reducing Oxidative Stress and Inhibiting Infiltration of Inflammatory Cells in an Allogeneic Stem Cell Transplantation Mouse Model. Med Sci Monit. 2018 Aug 27; 24:5973–9.

66. Lee JM, Moehlenkamp JD, Hanson JM, Johnson JA. Nrf2-Dependent Activation of the Antioxidant Responsive Element by tert-Butylhydroquinone Is Independent of Oxidative Stress in IMR-32 Human Neuroblastoma Cells. Biochem Biophys Res Commun. 2001 Jan;280(1):286–92.

67. Loboda A, Stachurska A, Florczyk U, Rudnicka D, Jazwa A, Wegrzyn J, et al. HIF-1 Induction Attenuates Nrf2-Dependent IL-8 Expression in Human Endothelial Cells. Antioxid Redox Signal. 2009 Jul;11(7):1501–17.

68. Johnson DA, Amirahmadi S, Ward C, Fabry Z, Johnson JA. The absence of the pro-antioxidant transcription factor Nrf2 exacerbates experimental autoimmune encephalomyelitis. Toxicol Sci Off J Soc Toxicol. 2010 Apr;114(2):237–46.

69. Murata H, Kunii H, Kusama K, Sakurai T, Bai H, Kawahara M, et al. Heat stress induces oxidative stress and activates the KEAP1-NFE2L2-ARE pathway in bovine endometrial epithelial cells. Biol Reprod. 2021 Nov 15;105(5):1114–25.

70. Feng J, He Y, Shen Y, Zhang G, Ma S, Zhao X, et al. Protective effects of nuclear factor erythroid 2-related factor on oxidative stress and apoptosis in the testis of mice before adulthood. Theriogenology. 2020 May; 148:112–21.

71. Fang F, Gong PS, Zhao HG, Bi YJ, Zhao G, Gong SL, et al. Mitochondrial modulation of apoptosis induced by low-dose radiation in mouse testicular cells. Biomed Environ Sci BES. 2013 Oct;26(10):820–30.

72. Wang R, Paul VJ, Luesch H. Seaweed extracts and unsaturated fatty acid constituents from the green alga Ulva lactuca as activators of the cytoprotective Nrf2–ARE pathway. Free Radic Biol Med. 2013 Apr; 57:141–53.

73. Twig G, Elorza A, Molina AJA, Mohamed H, Wikstrom JD, Walzer G, et al. Fission and selective fusion govern mitochondrial segregation and elimination by autophagy. EMBO J. 2008 Jan 23;27(2):433–46.

74. Yu B, Ma J, Li J, Wang D, Wang Z, Wang S. Mitochondrial phosphatase PGAM5 modulates cellular senescence by regulating mitochondrial dynamics. Nat Commun. 2020 May 21;11(1):2549.

75. Wang Z, Jiang H, Chen S, Du F, Wang X. The Mitochondrial Phosphatase PGAM5 Functions at the Convergence Point of Multiple Necrotic Death Pathways. Cell. 2012 Jan;148(1–2):228–43.

76. Li C, Lin L, Tsai H, Wen Z, Tsui K. Phosphoglycerate mutase family member 5 maintains oocyte quality via mitochondrial dynamic rearrangement during aging. Aging Cell. 2022 Feb;21(2):e13546.

77. Xu W, Jing L, Wang Q, Lin CC, Chen X, Diao J, et al. Bax-PGAM5L-Drp1 complex is required for intrinsic apoptosis execution. Oncotarget. 2015 Oct 6;6(30):30017–34.

8. Anex

8.1. Table of Figures

Figure 4.11	Melt curve of CA9 gene detected using real-time PCR. The figure shows a melting temperature of CA9 gene as 84.86°C with no amplifications detected in negative controls.
Figure 4.12	Relative expressions of AIFM1, KEAP1 and PGAM5 in scrotal hyperthermia group compared to the control group (***P<0.001 and ****P<0.0001). Data normalized to the expression of the housekeeping gene, β-actin.
Figure 4.13	Amplification plot of AIFM1 gene detected by real-time PCR. PCR cycles (X axis) were plotted against fluorescence intensity (Y axis).
Figure 4.14	Melt curve of AIFM1 gene detected using real-time PCR. The figure shows a melting temperature of AIFM1 gene as 82.47°C with no amplifications detected in negative controls.
Figure 4.15	Amplification plot of PGAM5 gene detected by real-time PCR. PCR cycles (X axis) were plotted against fluorescence intensity (Y axis).
Figure 4.16	Melt curve of PGAM5 gene detected using real-time PCR. The figure shows a melting temperature of PGAM5 gene as 84.56°C with no amplifications detected in negative controls.
Figure 4.17	Amplification plot of KEAP1 gene detected by real-time PCR. PCR cycles (X axis) were plotted against fluorescence intensity (Y axis).
Figure 4.18	Melt curve of KEAP1 gene detected using real-time PCR. The figure shows a melting temperature of KEAP1 gene as 87.09°C with no amplifications detected in negative controls.
Figure 4.19	Amplification plot of β-actin gene detected by real-time PCR. PCR cycles (X axis) were plotted against fluorescence intensity (Y axis).
Figure 4.20	Melt curve of β-actin gene detected using real-time PCR. The figure shows a melting temperature of β-actin gene as 84.86°C with no amplifications detected in negative controls.

8.2. List of Tables